LAWRENCE
LIVERMORE
NATIONAL
LABORATORY

LLNL-JRNL-801378

Low Molecular Weight Dissolved Organic Carbon: Aging, Compositional Changes, and Selective Utilization During Global Ocean Circulation

T. A. B. Broek, B. D. Walker, T. P. Guilderson, J. S. Vaughn, H. E. Mason, M. D. McCarthy

January 14, 2020

Global Biogeochemical Cycles

Disclaimer

Low Molecular Weight Dissolved Organic Carbon: Aging, Compositional Changes, and Selective Utilization During Global Ocean Circulation

Taylor A. B. Broek[1,2,*], Brett D. Walker[3,4], Thomas P. Guilderson[2], John, S. Vaughn[5], Harris E. Mason[5], and Matthew D. McCarthy[1]

[1]University of California, Santa Cruz, Ocean Sciences Department.
[2]Lawrence Livermore National Laboratory, Center for Accelerator Mass Spectrometry.
[3]University of Ottawa, Department of Earth and Environmental Science.
[4]University of California, Irvine, Department of Earth Systems Science.
[5]Lawrence Livermore National Laboratory, Center for Nuclear Magnetic Resonance Spectroscopy

*Corresponding author: Taylor Broek (broek1@llnl.gov)

Abstract

The composition and cycling dynamics of marine dissolved organic carbon (DOC) have received increase interest in recent years, however little research has focused on the refractory, low molecular weight (LMW) component that makes up the majority of this massive C pool. We measured stable isotopic ($\delta^{13}C$), radioisotopic ($\Delta^{14}C$), and compositional (C/N, ^{13}C solid-state NMR) properties of separately isolated high molecular weight (HMW) and LMW DOC fractions collected using a coupled ultrafiltration and solid phase extraction approach from throughout the water column in the North Central Pacific and Central North Atlantic. The selective isolation of LMW DOC material allowed the first investigation of the composition and cycling of a previously elusive fraction of the DOC pool. The structural composition of the LMW DOC material was homogeneous throughout the water column and closely matched carboxylic rich alicyclic material that has been proposed as a major component of the marine refractory DOC pool. Examination of offsets in the measured parameters between the deep waters of the two basins provides the first direct assessment of changes in the properties of this material with aging and utilization during ocean circulation. While our direct measurements largely confirm hypotheses regarding the relative recalcitrance of HMW and LMW DOC, we also demonstrate a number of novel observations regarding the removal and addition of DOC during global ocean circulation, including additions of fresh carbohydrate-like HMW DOC to the deep ocean and large-scale removal of both semi-labile HMW and recalcitrant LMW DOC.

1.0 Introduction

Marine dissolved organic carbon (DOC) is the largest pool of reduced and actively cycling carbon in the ocean. Early measurements of the radiocarbon age of DOC compared to that of dissolved inorganic carbon (DIC) demonstrated that at least a portion of DOC persists in the ocean on longer timescales than ocean circulation (Williams and Druffel, 1987; Druffel et al., 1992). These radiocarbon measurements combined with depth-based gradients in DOC concentration were used to form a two-pool model of DOC cycling, with a pool of semi-labile material that is produced in the surface and degraded or utilized on timescales less than ocean circulation and a background pool of refractory material that cycles on millennial timescales with a relatively conservative distribution throughout the water column. The semi-conservative behavior of DOC in the deep ocean has been utilized as a tracer to investigate transit times of different water-masses using offsets in radiocarbon age (Bauer et al., 1992; Hansell, 2013; Bercovici et al., 2018a; Druffel et al., 2019). However, DOC, even in the deep ocean, is a dynamic pool with constant removal and additions of new material (Smith et al., 1992; Hansman et al., 2009; Hansell and Carlson, 2013b; Walker et al., 2016a). Further, radiocarbon measurements of different components of the DOC pool have demonstrated a remarkable heterogeneity of $\Delta^{14}C$ values (Walker et al., 2011; Walker et al., 2014; Zigah et al., 2017; Broek et al., 2017) ranging from above modern (Druffel and Beaupré, 2009; Repeta and Aluwihare, 2006) to tens of thousands of years (Ziolkowski and Druffel, 2010; Coppola et al., 2015), suggesting substantial variability in recalcitrance and cycling rates.

Increasing evidence has demonstrated a relationship between the average molecular weight of DOC, its radiocarbon content, and the relative recalcitrance of the material (Walker et al., 2011; Benner and Amon, 2015; Walker, et al., 2016a; Walker et al., 2016b; Broek et al., 2017). High molecular weight (HMW) DOC is primarily composed of recently produced material and contains intact biochemicals, whereas low molecular weight (LMW) DOC is old, degraded, biologically refractory, and dominates the background DOC pool that persists in the ocean on millennial timescales (Amon and Benner, 2015). The LMW fraction of the DOC pool is therefore a critical component that stores the vast majority of the ocean's dissolved organic carbon and nitrogen.

Until recently there has been no analytical approach to directly investigate the refractory LMW DOC pool. The analyses that are possible in total seawater, primarily concentration measurements and bulk isotopic analyses, are limited and interpretations based on these measurements are impacted by the extreme heterogeneity of marine DOC. Material

concentrated using ultrafiltration (UDOM) has been widely used for many DOC investigations. However, this is by definition HMW and therefore not representative of the refractory DOC pool. New generations of solid phase extraction (SPE) sorbents have more recently been used to isolate DOC that, based on high resolution mass spectrometry analyses (e.g., FT-ICR MS), has been largely interpreted as primarily LMW material. However, it has been recently demonstrated that SPE-DOM isolated from whole seawater contains a fraction of younger, more labile HMW material (Broek et al., 2017). Coupled with ^{14}C ages that are comparable to total DOC (Flerus et al., 2012; Lechtenfeld et al., 2014; Bercovici et al., 2018b), these new observations suggest SPE isolates are more similar to total DOC than LMW DOC. The diversity of molecules with varying ages and biological reactivities in SPE-DOM therefore complicates interpretation of the composition and cycling dynamics of LMW DOC (Broek et al., 2017). An alternate approach to the study of LMW DOC has been indirect observations from the differences between ultrafiltered HMW DOC and total DOC. A number of studies have inferred properties of the LMW DOC pool, such as ^{14}C age from these indirect calculations. However, these analyses are also severely limited by what it is possible to measure in whole seawater (Loh et al., 2004; Kaiser and Benner, 2009). Without a method to selectively isolate LMW DOM, it has not been possible to directly apply many analyses with vast informational potential such as NMR and molecular level analyses requiring large sample sizes. Overall, this has limited our understanding of the broad functional composition of DOC.

Here we present data from samples collected via a new DOC isolation approach using sequential ultrafiltration and SPE as an effective means to isolate both young, HMW DOC and old, LMW DOC from seawater (Broek et al., 2017). By collecting these distinct fractions, thereby limiting the influence of DOC size and reactivity mixtures, this combined UF/SPE method provides a more direct approach than has previously been possible to investigate the composition, sources, and cycling of the most refractory material in the ocean. For the first time we measure the stable isotope ratios, elemental composition, and molecular composition of selectively isolated LMW DOC from throughout the water column in both the Atlantic and Pacific Ocean Basins. We interpret the results in the context of radiocarbon age and offsets between basins to determine how the properties of this material change during deep ocean circulation. The isotopic and molecular composition of the LMW fraction and basin offsets in these properties are compared to the more commonly studied semi-labile HMW UDOM material, collected from the same water, in order to investigate the relative behavior of different components of the DOC size and reactivity spectrum. Together these represent the first

comprehensive look at compositional changes of both semi-labile and refractory DOC with aging and utilization during large scale ocean circulation.

2.0 Materials and Methods

2.1 Sample Collection

Samples were collected on four research cruises aboard the R/V Kilo Moana in August 2014 and May 2015 and the R/V Atlantic Explorer in August 2015 and May 2016. Sampling was conducted at the Hawaii Ocean Time Series (HOT) Station ALOHA (A Long-Term Oligotrophic Habitat Assessment; 22° 45'N, 158° 00'W) in the North Central Pacific (NCP) and the Bermuda Atlantic Time Series Site (BATS; 31° 40'N, 64° 10'W) in the Central North Atlantic. Surface water was sampled via the vessels' underway sampling systems with an inlet at approximately 7.5 m water depth on the R/V Kilo Moana and 2 m water depth on the R/V Atlantic Explorer. The laboratory seawater taps were flushed for approximately 2 hours prior to each sampling. Large volume subsurface water samples were collected from 400 m, 850 m, and 2500 m using successive casts of a rosette equipped with 24 x 12 L Niskin bottles. Seawater was pre-filtered through 53 µm Nitex mesh and pumped through 0.2 µm polyethersulfone (PES) cartridge filters prior to ultrafiltration. All filters and storage containers were cleaned with 10% HCl and ultrapure water (Milli-Q; 18.2 MΩ) then flushed with seawater from the sampling depth prior to use.

2.2 DOC Isolation

A detailed explanation of the DOC isolation protocol is described in Broek et al. (2017). Briefly, ultrafiltration was performed using a custom-built system consisting of four-spiral wound PES UF membranes (2.5 kD; GE Osmonics GH2540F30, 40-inch long, 2.5-inch diameter) mounted in stainless steel housings, plumbed in parallel to a 100 L fluorinated HDPE reservoir, with flow driven by a 1.5 HP stainless steel centrifugal pump. Seawater samples of 1000-4000 L were concentrated to a final retentate volume of 15-20 L, then further reduced to 2-3 L with a second custom-built ultrafiltration system with a single membrane of a smaller MW cutoff (1 kD GE Osmonics GE2540F30, 40-inch long, 2.5-inch diameter, 1 kD MWCO), Samples were then desalted by continuously adding 40 L of Milli-Q water at the same rate of membrane permeation. UDOM samples were dried to powder with a combination of rotovap and centrifugal evaporation. LMW DOC permeating the UF system was isolated using PPL sorbent (Agilent Bondesil PPL, 125 µm particle size, part # 5982-0026) following the general recommendations

of Dittmar et al. (2008) and Green et al. (2014), including loading rates, seawater to sorbent ratios, and elution volumes and rates. Permeate from the UF system was acidified in 200 L batches to pH 2 with HCl and pumped through the SPE sorbent contained in a parallel combination of 2 medium-pressure glass chromatography columns equipped with 0.2 µm quartz fiber filters at the column inlet to prevent biofouling and remove any particulate contaminants from the UF permeate. Following sample loading, the SPE sorbent was desalted with 6 L of pH 2 ultrapure water. The LMW SPE-DOM material was eluted with six 500 mL additions of methanol that was similarly dried to powder via rotovap and centrifugal evaporation.

2.3 Total DOC ([DOC], [DON], $\Delta^{14}C$, $\delta^{13}C$)

Subsamples for dissolved organic carbon (DOC) and total dissolved nitrogen (TDN) concentration measurements were collected into pre-combusted 40 mL borosilicate glass vials following 0.2 µm-filtration. DOC and TDN concentration measurements were made via the high-temperature catalytic oxidation method using a Shimadzu TOC-V analyzer in either the Carlson lab at University of California, Santa Barbara (https://labs.eemb.ucsb.edu/carlson/craig/services) or the Benner lab at the University of South Carolina (Benner et al., 1993). DOC concentrations measurements were also determined via UV oxidation, cryogenic purification, and manometric determination at UC Irvine (Beaupré et al., 2007; Walker et al., 2019). DOC concentrations were similar between the two methods and the presented values represent the error weighted average of both measurements and uncertainties represent the propagated instrumental uncertainty of each method. Total DON concentrations were determined by subtracting the sum of dissolved inorganic nitrogen (DIN) species (nitrate, nitrite, ammonia) concentrations, determined using a Lachat QuickChem 8000 Flow Injection Analyzer, from the measured TDN concentrations. Seawater samples for C isotopic analysis ($\delta^{13}C$, $\Delta^{14}C$) were collected, following 0.2 µm filtration, into pre-combusted 1000 mL Amber Boston Round bottles, immediately frozen, and stored at -20°C. At BATS, total DOC samples for concentration and isotopic analyses were collected only during the May sampling period.

2.4 EA-IRMS ($\delta^{13}C$, C/N)

Stable carbon isotope ratios ($\delta^{13}C$) and elemental ratios $(C/N)_a$ were determined via elemental analyzer isotope ratio mass spectrometry (EA-IRMS) at the University of California, Santa Cruz, Stable Isotope Laboratory (UCSC-SIL; http://emerald.ucsc.edu/~silab/) using a Carlo Erba CHNS-O EA1108-elemental analyzer interfaced via a ConFlo III device with a ThermoFinnigan Delta Plus XP isotope ratio mass spectrometer (Thermo Fisher Scientific). Standards, EA-IRMS protocols, and correction routines followed standard UCSC-SIL protocols.

Analytical uncertainties of n=3 replicate measurements of the $\delta^{13}C$ of isotopic standards ranged from ± 0.05 to 0.1‰.

2.5 ^{14}C-AMS ($\Delta^{14}C$)

Natural abundance radiocarbon (^{14}C) determinations of all isolated fractions were performed at Lawrence Livermore National Laboratory, Center for Accelerator Mass Spectrometry (LLNL-CAMS) by AMS following standard graphitization procedures (Vogel et al., 1984; Santos et al., 2007). The radiocarbon content of total DOC (<0.2 µm) was determined by UV-oxidation at the UC Irvine Keck Carbon Cycle AMS Lab (Beaupré et al., 2007; Griffin et al., 2010; Walker et al., 2019). Results are reported as age-corrected $\Delta^{14}C$ (‰) for geochemical samples and have been corrected to the date of collection and are reported in accordance with conventions set forth by Stuiver and Polach (1977). The isotopic values are reported as background and $\delta^{13}C$ corrected fraction modern (Fm), $\Delta^{14}C$, and conventional radiocarbon age (ybp).

2.6 Solid-state ^{13}C NMR

Solid state ^{13}C {^{1}H} cross polarization magic angle spinning (CP/MAS) NMR spectra were collected on a Bruker Avance III spectrometer operating at 100.5474 MHz for ^{13}C and 399.8285 MHz for ^{1}H. A Bruker HXY MAS probe was used, along with 4 mm ZrO2 rotors with Kel-F tips. The ^{1}H π/2 pulse was 4 µs, and cross polarization was achieved via a 70-100% power ramp on the ^{1}H nucleus. Cross polarization contact time was 4 ms, and the MAS rate was 10 kHz. The ^{13}C power (62.5 kHz) and SPINAL-64 ^{1}H decoupling (225 kHz) were optimized using the peak intensity and peak widths of glycine, and ^{13}C chemical shifts were measured relative to the carboxylic acid group on glycine at ^{13}C = 176.49 ppm. A total of 16,384 acquisitions were collected for each sample with a 1 s pulse delay. 512 points were used for Fourier transform with a 10 µs dwell time. 100 Hz of line broadening was applied during processing.

The relative distribution of different functional groups was determined by integrating the area under the curve using the chemical shift ranges and assignments from Mao et al., 2012 as follows (Supplemental Fig. 2): ketone, aldehyde, quinone (220-191 ppm); COO, NC=O (191-164 ppm); aromatic C-O (164-150 ppm); aromatics (150-117 ppm); OCO (94-60 ppm); OC (94-60 ppm); OCH3, NCH (60-45 ppm); CCH2C, CCHC (45-30 ppm); CCH2C, CCH3 (30-0 ppm). For some comparisons, including to previous data, regions were combined (as in Koprivnjak et al., 2009), resulting in four generalized groupings (Fig. 4): carboxyl C (220-164 ppm), aromatic C (164-117 ppm), alkoxy C (117-60 ppm), and alkyl C (60-0 ppm).

Because different functional groups produce varying responses, this spectroscopic technique is not completely quantitative, and reported distributions represent the distribution of spectroscopic signal associated with each functional group rather than the absolute concentration. However, all spectra were collected under identical conditions, allowing the direct comparison of these relative distributions between samples. All spectra were normalized to the total area for comparison and for the calculation of difference spectra.

2.7 Non-retained DOC mass balance calculations and error propagation

The elemental ratios (C/N) and carbon isotopic values ($\delta^{13}C$, $\Delta^{14}C$) of the DOM not isolated by the combined UF/SPE method (the non-retained pool; NR) were calculated by subtracting the properties of both the HMW UDOM and LMW SPE-DOM fractions from those of the total DOM pool. For carbon isotopic values, this was calculated using a simple mass balance calculation:

$$\boldsymbol{X_{NR}} = \frac{([\boldsymbol{Total\ DOC}] * \boldsymbol{X_T}) - ([\boldsymbol{HMW\ UDOC}] * \boldsymbol{X_{HMW}}) - ([\boldsymbol{LMW\ SPEDOC}] * \boldsymbol{X_{LMW}})}{[\boldsymbol{Total\ DOC}] - [\boldsymbol{HMW\ UDOC}] - [\boldsymbol{LMW\ SPEDOC}]}$$

Where *X* represents the isotopic value of the specific fractions / pools. The uncertainties associated with the non-retained value were determined by propagating the errors associated with both the concentration of each fraction and the instrumental measurement error for each isotopic value using the equations described in Taylor (1997) for the calculation of uncertainties in functions of several variables. The uncertainties in the recovered mass of the HMW UDOC and LMW SPE-DOC used to calculate the concentration of each fraction was assumed to be ± 10%, encompassing the error associated with sample weighing and potential losses during sample transfers. The average uncertainty of the total DOC concentration measurements was ± 3 µmol L^{-1}, encompassing the measurement error of 2 separate methods as described in section *2.3*.

The C/N ratio of the non-retained DOM was determined by separately calculating the molar concentration of [DOC] and [DON] in the non-retained pool by difference:

$$\boldsymbol{C/N_{NR}} = \frac{[\boldsymbol{Total\ DOC}] - [\boldsymbol{HMW\ UDOC}] - [\boldsymbol{LMW\ SPEDOC}]}{[\boldsymbol{Total\ DON}] - [\boldsymbol{HMW\ UDON}] - [\boldsymbol{LMW\ SPEDON}]}$$

The uncertainties of non-retained C/N values were calculated by propagating the uncertainties associated with the concentration measurements (± 10% for the HMW UDOM and LMW SPE-DOM fractions). The average uncertainty of the total DOC and total DON concentrations used in these calculations were ± 3 µmolC L^{-1} and ± 1 µmolN L^{-1} respectively.

225

226

227 **3.0 Results**

228 *3.1 DOC Concentration and Recovery of High and Low Molecular Weight DOC Fractions*

229 DOC concentrations in the Central North Atlantic are highest at the surface (average =
230 84 ± 14 µM) with offsets between August (94 ± 5 µM) and May (74 ± 8 µM) sampling (Fig. 1a).
231 The concentration decreases through the upper 850 m to a relatively constant deep ocean
232 concentration of 48 ± 2 µM (Average ≥ 850 m). In the NCP, DOC concentrations are lower
233 throughout the water column with an average surface concentration of 78 ± 3 µM decreasing to
234 a deep ocean (2500 m) value of 37 ± 3 µM. There is some seasonal variability in surface ocean
235 concentration, however, to a lesser degree than in the Atlantic Basin (August = 80 ± 1 µM; May
236 = 76 ± 1 µM).

237 In the Central North Atlantic, ultrafiltration recovered an average of 10 µmol-C L^{-1} in the
238 surface and 5 µmol-C L^{-1} in the subsurface (≥ 400 m), representing 12 ± 1 % and 9 ± 1 % of
239 total DOC respectively (Fig. 1b). In the NCP, ultrafiltration recovered 13 µmol-C L^{-1} in the
240 surface and 4 µmol-C L^{-1} in the subsurface (≥ 400 m), representing 17 ± 1 % and 9 ± 1 % of
241 total DOC respectively. At 2500 m there is a significant difference in the HMW UDOC
242 concentration between basins ($t = 4.74$; $df = 10$; $p < 0.001$)

243 SPE of LMW DOC permeating the ultrafiltration system recovered 22 µmol-C L^{-1} from
244 surface waters of the Central North Atlantic and an average of 17 µmol-C L^{-1} from subsurface
245 waters (≥ 400 m; Fig 1c). SPE recovered less material from the NCP, isolating 15 µmol-C L^{-1} in
246 the surface and an average of 12 µmol-C L^{-1} in the subsurface (≥ 400 m). Although the recovery
247 in the surface was slightly higher than in the subsurface (≥ 400 m), as a result of the decreasing
248 concentration of total DOC with depth, the relative % recovery is lower in the surface and higher
249 at depth. In the Central North Atlantic this recovery represents 26 ± 3 % of total DOC in the
250 surface and 34 ± 3 % in the subsurface (≥ 400 m). In the NCP the DOC recovery represents 18
251 ± 2 % of total DOC in the surface and 29 ± 2 % in the subsurface (≥ 400 m). At 2500 m there is
252 a significant difference in the LMW SPE-DOC concentration between basins (Fig 1c; $t = 18.01$;
253 $df = 10$; $p < 0.001$).

254 *3.2 Radiocarbon ($\Delta^{14}C$) of total, HMW, and LMW DOC*

255 In the Central North Atlantic the surface $\Delta^{14}C$ value of total DOC is -186 ± 4 ‰ (1590

ybp; May sampling only) and decreases through the water column to a minimum value of -438 ± 4 ‰ (4570 ybp) at 850 m (Fig. 2a). There is a slight increase in $\Delta^{14}C$ at 2500 m ($\Delta^{14}C$ = -392 ± 4 ‰; 3930 ybp). In the NCP, the $\Delta^{14}C$ of total DOC is depleted (older ^{14}C age) at all depths, with an average surface value of -227 ± 14 ‰ (2000 ybp) decreasing to a minimum in the deepest samples (2500 m; -544 ± 10 ‰; 6240 ybp). We note that samples for total DOC radiocarbon analysis were only collected at BATS during the May sampling season. It is likely that there would be a difference in the $\Delta^{14}C$ values of DOC in surface waters between the two sampling periods, presumably with younger values when concentrations are higher due to the accumulation of fresh DOC in stratified surface waters. However, if the surface $\Delta^{14}C$ offset within the 2 fractions is considered, the offset in total DOC $\Delta^{14}C$ between the two seasons would be on the order 20 ‰. A seasonal difference on the order of 20‰ with an uncertainty in these measurements on the order of 5-10 ‰ would be insignificant.

HMW UDOC $\Delta^{14}C$ values are enriched (younger ^{14}C age) relative to that of total DOC throughout the water column in both basins (Fig. 2b) with an average value of -54 ± 15 ‰ (440 ybp) in the surface of the Central North Atlantic decreasing to a minimum in the deepest samples (2500 m; -278 ± 16 ‰; 2630 ybp). In the NCP, the average surface $\Delta^{14}C$ of HMW UDOC is similar to surface waters in the Central North Atlantic (-45 ± 10 ‰; 300 ybp), however, is depleted throughout the rest of the water column, with a minimum of -375 ± 10 ‰ (3700 ybp) in the deepest samples (2500 m). There is a significant offset in HMW DOC $\Delta^{14}C$ between basins at 2500 m ($t = 9.86$; $df = 10$; $p < 0.001$).

In contrast, the $\Delta^{14}C$ of LMW SPE-DOC is depleted (older ^{14}C age) relative to total DOC throughout the water column in both basins (Fig. 2c). In the Central North Atlantic, the $\Delta^{14}C$ value of LMW SPE-DOC mirrors that of total DOC with an average value of -323 ± 12 ‰ (3120 ybp) in the surface, decreasing to a minimum at 850 m (-467 ± 23 ‰; 5050 ybp), with a slight increase in the 2500 m samples ($\Delta^{14}C$ = -437 ± 37 ‰; 4530 ybp). In the NCP, the average $\Delta^{14}C$ of LMW SPE-DOC is depleted relative to the Central North Atlantic throughout the water column with an average surface value of -350 ± 9 ‰ (3380 ybp) decreasing to a minimum of -573 ± 6 ‰ (6770 ybp) in the deepest samples (2500 m). There is a significant offset in LMW SPE-DOC $\Delta^{14}C$ between basins at 2500 m ($t = 9.69$; $df = 10$; $p < 0.001$).

The average $\Delta^{14}C$ of the non-retained DOC (Fig. 2d) is equivalent within error to total DOC throughout the water column in both basins (average offset = 14 ‰). As such, this is also equivalent to the mass weighted sum of the HMW UDOC and LMW-SPE DOC fractions, demonstrating the representativeness of the two combined fractions relative to total DOC.

3.3 DOC Composition

3.3.1 Elemental (C/N) Composition

Carbon to nitrogen atomic ratios $(C/N)_a$ of total DOM, HMW UDOM, and LMW SPE-DOM are distinct from each other throughout the water column (Fig. 3a-c). The average C/N ratio of total DOM in all samples is 16 ± 4, however, within each sample the average standard deviation is high due to the compounded error associated with the high uncertainty of [DOC] and [DON] values (Fig. 3a). As a result, there is no depth structure in either basin. However, in the deepest sample (2500 m) there is an offset between the two basins, with higher values in the NCP (18 ± 3) than the Central North Atlantic (11 ± 2). The C/N ratio of HMW UDOM is lower on average than total DOM and has a narrow range of values (11 to 14), with no depth structure or offsets between basins (Fig. 3b). In contrast, the C/N ratio of LMW SPE-DOM is higher than both total DOM and HMW DOM (Fig. 3c). The ratio is highest in the surface and decreases through the upper water column. At 2500 m there is a significant offset in the C/N ratio ($t = 4.41$; $df = 10$; $p \leq 0.01$), with higher values in the NCP (24 ± 2) than the Central North Atlantic (28.5 ± 1.5).

3.3.2 Stable Isotopic ($\delta^{13}C$) Composition

The $\delta^{13}C$ of total DOC has a narrow range of values (-22.7 to -21.1 ‰) that are indistinguishable within error throughout the water column between the Central North Atlantic and NCP (Fig. 3e). There is some depth structure in both basins with the most enriched values in the surface (average of both basins = -21.1 ± 0.4 ‰) and more depleted values in the subsurface (average of all depths ≥ 400 m in both basins = -22.1 ± 0.4 ‰). Similar to total DOC, there are no offsets in HMW UDOC $\delta^{13}C$ values between basins (Fig. 3f). There is depth structure in HMW UDOC $\delta^{13}C$ values that follows the opposite trend of total DOC, with the most depleted values in the surface (average of both basins = -22.4 ± 0.1 ‰) and enriched values in the subsurface (average of all depth ≥ 400 m in both basins = -21.5 ± 0.25 ‰). In the surface HMW UDOC values are depleted relative to total DOC but are enriched relative to total DOC in the subsurface. In contrast, the $\delta^{13}C$ of LMW SPE-DOM has a narrow range of values that are depleted relative of both total DOC and HMW UDOC throughout the water column (Fig. 3g; average of all samples = -22.7 ± 0.3 ‰). Similar to HMW UDOC, LMW SPE-DOM $\delta^{13}C$ values are most depleted in the surface (average of both basins = -22.9 ± 0.2 ‰) and increase with depth (average at 2500 m = -22.5 ± 0.3 ‰). There is a basin offset in the upper 850 m (average offset = 0.3 ‰), but no offset in the 2500 m sample.

3.3.3 Functional Composition (Solid State ^{13}C-NMR)

The ^{13}C {^{1}H} CP/MAS NMR spectra of HMW UDOC are dominated by peaks at ~110 ppm (acetal; O-C-O) and ~80 ppm (alkyl O-C-H) (Fig. 4a; Supplemental Fig. 2). The average ratios of O-alkyl to acetal C in HMW UDOC is 5.4 ± 1.0, consistent with the ratios of typical carbohydrates (Sannigrahi et al., 2005). This alkoxy component has the greatest relative abundance in the surface, comprising an average of 62 ± 3 % of the total signal, and is attenuated at depth (2500 m; 47 ± 2 %). The remainder of the signal is comprised of carboxyl (~175 ppm; 13 ± 5 %), and aliphatic (0-60 ppm; 31 ± 4 %) functional groups, with a minor aromatic (~135 ppm; ~1 %) component.

In contrast, the LMW SPE-DOC spectra are dominated by aliphatic (0-60 ppm; 62 ± 3 %) and carboxyl (~175 ppm; 16 ± 1 %) functionality (Fig. 4b; Supplemental Fig. 2). There is also a greater proportion of aromatic C (~135 ppm; 4 ± 1 %) in the LMW fraction. The signal in the alkoxy region (117-60 ppm; i.e. carbohydrate C in HMW DOC) comprises 17 ± 2 % of the LMW signal, however this is almost entirely O-alkyl C and therefore the ratio of the O-alkyl to acetal C is much higher (32 ± 12) than in the HMW fraction. Unlike the HMW material, there is little variability in relative proportion of functional groups with depth or between basins.

4.0 Discussion

4.1 Composition of LMW SPE-DOC and comparison to HMW UDOC

4.1.1 Elemental and Isotopic Composition.

The novel LMW DOC fraction recovered by our combined UF/SPE isolation approach allows for an examination of the composition of the refractory material that is thought to persist in the ocean on millennial timescales. While the LMW material collected in the NCP has previously been characterized (Broek et al., 2017), the addition of material from a second basin confirms a number of hypotheses that were suggested by more limited data, while also providing more mechanistic interpretations.

Radiocarbon analysis of the LMW material shows an average age that is older than both the total DOC pool and the HMW UDOC fraction, indicating that it represents a slower cycling component of marine DOC (Benner and Amon, 2015; Fig. 2). The LMW material has C/N ratios that are elevated compared to the total pool, suggesting that LMW DOC throughout the water column is C-rich, consistent with expectations for the alicyclic and lipid derived material that has

been hypothesized to account for a considerable portion of recalcitrant marine DOC (Hwang, 2003; Hertkorn et al., 2006; Koprivnjak et al., 2009; Fig. 3c).

With the addition of the Central North Atlantic study site, we can now confirm a decrease in the C/N ratio of the LMW fraction through the upper water column (Fig. 3c). This finding is unexpected as it suggests that a nitrogenous component exists within the LMW pool that could be more refractory than some portion of the non-N-containing material. However, while contrary to expectations based on common assumptions about the relative lability of N-containing materials, this observation is consistent with the depth related changes in $\delta^{13}C$ of the LMW material (Fig. 3g). Overall, the $\delta^{13}C$ values of LMW DOC are depleted relative to the total DOC pool in both basins that was previously hypothesized to correspond to a contribution from ^{13}C depleted lipid-like material (Hayes, 2001; Broek et al., 2017). However, the $\delta^{13}C$ values are also variable through the water column in both basins and values become more enriched with depth, coincident with the observed changes in C/N ratio. A least squares linear regression model of $\delta^{13}C$ and C/N ratio shows a strong relationship ($R^2 = 0.53$, p-slope < 0.001) in both basins, especially when considered in each basin separately (Atl. $R^2 = 0.94$, p-slope < 0.001; Pac. $R^2 = 0.77$, p-slope =0.0047; Supplemental Fig. 1).

We hypothesize that these observations can be explained by changes in the relative contribution of different major compound types. Specifically, in contrast to the ^{13}C depleted values of lipid material, N-containing materials known to be present in the marine environment, such as peptides and tetrapyrroles compounds, all have elevated $\delta^{13}C$ compared to most other compound classes (Hayes, 2001). While there are no published data on N functionality of the LMW pool, there is at least some evidence to suggest that pyrrol and indol containing compounds may be more important than is currently recognized. For example, hydrolyzable amino acids make up most N in reactive surface DON, however these are a minor component of LMW DON (Kaiser and Benner, 2009; Benner and Amon, 2015). At the same time, solid state NMR of HMW DON indicates increasing heterocyclic-N functionality in the deep ocean (McCarthy et al., 1997; Aluwihare and Meador., 2008; Mao et al., 2012), representing old material where HMW and LMW structural compositions may begin to overlap. This evidence suggests that refractory heterocyclic-N material may be an important component of LMW DON, and also that more rapid remineralization of a labile, C-rich, lipid-like material could be more important than is currently understood. Together, this could explain the observed trends in both the C/N ratio and $\delta^{13}C$ of the LMW fraction.

Finally, an additional implication of these observations is that there must be some amount of active cycling occurring within the LMW DOC pool, even in the subsurface ocean,

386 despite its old average ^{14}C age. This is also required, given the ^{14}C depth trends observed
387 within this fraction (Fig. 2c). The average ^{14}C age of LMW SPE-DOC material in the surface
388 ocean is thousands of years younger than LMW SPE-DOC in the deep ocean, clearly
389 demonstrating that there is a fraction of more rapidly cycling LMW material in the surface ocean
390 that is not present in the deep ocean. However, given that in the subsurface ocean most DOC is
391 LMW, this is not necessarily an unexpected observation.
392 In contrast, the bulk properties of the more commonly studied HMW UDOC material is
393 unique relative to the LMW SPE-DOC fraction collected from the same water. As mentioned
394 above, the average age of the HMW fraction is significantly younger than both the total DOC
395 pool and the LMW fraction throughout the water column in both basins, suggesting that this
396 fraction represents a faster cycling component of the marine DOC pool (Benner and Amon,
397 2015; Broek 2017). This is consistent with previous measurements of ultrafiltered material,
398 bioassay experiments, and expectations based on observed size-age relationships (Benner et
399 al., 1997; Walker et al., 2011; Broek et al., 2017; Shen and Benner, 2019). The C/N ratio of the
400 HMW material is also lower than that of the LMW material and consistent throughout the water
401 column in both basins. This was previously interpreted in the NCP as evidence that the
402 youngest, most labile fraction of the DOC pool has a relatively uniform N-content, likely due to
403 rapid and non-selective remineralization (Broek et al., 2017). However, despite the lack of depth
404 trend in C/N ratio within the HMW pool in either basin, there is a depth trend in $\delta^{13}C$ values.
405 When looking at both basins together, it is clear that this trend mirrors a similar trend in the
406 LMW pool, with the lowest values in the surface and an increase with depth. The depleted $\delta^{13}C$
407 value of HMW DOC in the surface was previously hypothesized to be evidence of a relatively
408 labile HMW ^{13}C-deplete component (Broek et al., 2017), but the low C/N ratios and lack of C/N
409 depth trend in the HMW fraction is inconsistent with the C-rich nature of the most likely
410 candidate compounds, such as lipids. However, because the $\delta^{13}C$ of lipid-like material can have
411 considerably depleted values (Hayes, 2001) a small contribution from this material in the
412 surface ocean could greatly skew the high $\delta^{13}C$ values of the HMW fraction but have little effect
413 on the C/N ratio. Because these more labile lipid compounds are likely to be actively degraded
414 in the surface ocean, it is plausible that their degradation products would be present as both
415 HMW structures and LMW degradation products, potentially decreasing the $\delta^{13}C$ value of
416 surface material in both MW fractions. Alternately, it is possible that the lack of C/N variability in
417 the HMW fraction despite the $\delta^{13}C$ depth trends could be caused by a labile N-containing lipid
418 component, such as lipopeptides that have been confirmed to be present in surface waters
419 (Kaiser and Benner, 2008) and would likely be HMW (Broek et al., 2019).

4.1.2 NMR functional composition

Solid-state ^{13}C NMR analysis is a powerful tool for determining the C functional composition of isolated DOC fractions. While both HMW UDOC (Benner et al., 1992; McCarthy et al., 1993; Sannigrahi et al., 2005; Hertkorn et al., 2006) and material isolated with reverse osmosis electro dialysis (RO/ED; Koprivnjak et al., 2009; Mao et al., 2012) have been characterized by this approach previously, our isolated LMW SPE-DOC fraction provides a direct view of material that is either absent (in HMW UDOC), or likely to be obscured in a complex mixture by the presence of semi-labile HMW material (in RO/ED material).

The functional composition of our LMW SPE-DOC fraction is considerably different from that of these previous solid-state NMR measurements. The signal is dominated by alkyl C, with a substantial amount of highly saturated aliphatic functionality. There is also a large contribution from carboxyl C and a larger aromatic component than seen in HMW UDOC. There is some additional signal from alkoxy C, however, the high ratio of O-alkyl to acetal C suggests that this signal is almost certainly not derived from polysaccharides as is hypothesized for HMW DOC, but rather other more complex hydroxyl containing structures. When area normalized to the total signal, the four LMW DOC spectra collected for this study, representing material from the surface and deep ocean (2500 m) in both Atlantic and Pacific Basins, are identical within the limits of this technique (Fig. 4b). This is strongly consistent with our ^{14}C data, indicating that in both the surface and deep ocean, our isolated LMW fraction represents a persistent refractory component with long oceanic residence times that is well mixed throughout the water column and world ocean.

The functional composition of HMW UDOC from the same waters is generally consistent with previous measurements of ultrafiltered material (Supplemental Fig. 3a; Benner et al., 1992; McCarthy et al., 1993; Sannigrahi et al., 2005), and provides useful contrast with our new LMW fraction. In the surface ocean, where the signal is dominated by alkoxy C, thought to primarily represent polysaccharide containing compounds, spectra are essentially identical to those published previously. There is a decrease in the relative proportion of the alkoxy C signal between the surface and deep ocean within the HMW fraction in both basins (Fig. 7a), also consistent with prior observations. This has been interpreted to represent a highly reactive labile fraction that is preferentially degraded (Repeta and Aluwihare, 2006). Further, the ratio of O-alkyl to acetal C of the material that is present in the surface but absent at depth is approximately 4 ± 1, confirming that the removed material is likely dominated by polysaccharides (Sannigrahi et al., 2005). There is no disappearance of other functional groups with depth, suggesting that the more refractory material within the HMW pool is dominated by

alkyl C.

Direct NMR measurements of DOC isolated by RO/ED that, on average, isolates far more material (70-80% of total DOC; Vetter et al., 2007) than either UF or SPE alone, show a compositional intermediate between our two fractions (Supplemental Fig. 3c; Koprivnjak et al., 2009; Mao et al., 2012). This is expected, as this material contains a larger fraction of total DOC and therefore represents a mixture of LMW and HMW material. Therefore, on a bulk structural level, the largest DOC fraction ever isolated (by RO/ED) is a mixture of two or more compositionally distinct pools. This observation, coupled with our radiocarbon and elemental composition data, arguably indicates that efforts to isolate the entire DOC pool can confound interpretations.

Beyond general composition, the specific functional distributions of our LMW SPE-DOC, dominated by alkyl and carboxyl peaks, is also remarkably similar to the functional distribution of the proposed carboxyl-rich alicyclic molecule (CRAM) fraction of DOC (Hertkorn et al., 2006). CRAM is hypothesized to be distributed throughout the ocean at all depths, be present in all MW fractions, and represent a major refractory component of marine DOC. The proposed functional composition of this material was based on two different solid-state NMR based approaches. CRAM was first proposed by calculating the difference between deep ocean and surface UDOC spectra, revealing a component dominated by carboxyl and alkyl C with a smaller contribution from aromatic C (Hertkorn et al., 2006), and later by a similar approach subtracting the spectra of UDOC from RO/ED spectra in order to visualize the component of the DOC pool not isolated by ultrafiltration (Koprivnjak et al., 2009). These visualizations closely matched that of the hypothetical CRAM fraction and suggested that CRAM is in fact a dominant component of the background refractory pool of DOC. More important, these subtractions resulted in spectra identical to that of our LMW SPE-DOM fraction (Supplemental Fig. 3b), providing further evidence that our LMW material is functionally representative of the whole LMW DOC pool and confirms that our LMW DOC fraction allows the first direct means to investigate the composition and cycling of this major DOC pool. The presence and dominance of CRAM material within the refractory LMW pool is consistent with the relative homogeneity of the functional composition our LMW DOC fraction at all depths and in both basins.

Finally, the identification of CRAM material within the HMW pool, both by previous studies and in this data (Supplemental Fig. 4), combined with the dominance of CRAM in our LMW fraction shows that CRAM in fact spans a large range of MW. Combined with the large range of ^{14}C ages of our DOC fractions and specifically the LMW material, this observation suggests that much of the CRAM material that dominates the background DOC pool, is likely

produced directly in the surface ocean, in addition to being produced by successive microbial reprocessing and degradation throughout the water column. This challenges the hypothesis that LMW DOC comes primarily from the decomposition of HMW DOC and that microbial degradation is the main driver shaping size-reactivity relationships.

4.2 Changes in deep ocean DOC during ocean circulation

The waters at 2500 m at the BATS and HOTS sites are within the North Atlantic Deep Water and Pacific Deep Water water-masses respectively. If these water-masses are interpreted as upstream and downstream endmembers of deep ocean circulation, differences in the concentration and properties of DOC between basins provides a direct means of investigating the utilization of DOC over the millennial timescales associated with deep water movement (DeVries and Primeau, 2011; Hansel, 2013b; Bercovici et al., 2018; Druffel et al., 2019).

At 2500 m there is a 11 ± 3 µM offset in total DOC concentration between basins, demonstrating deep removal of approximately 25% of total DOC during ocean circulation (Fig. 6a). This observation is similar to independent prior estimates (e.g., ~14 µmol kg-1; Hansell, 2013). Within the individual fractions the offset is 1.3 ± 0.7 µM for HMW UDOC and 5.2 ± 0.7 µM for LMW SPE-DOM, representing approximately 10% and 45% of the total remineralized DOC respectively. This indicates that a large proportion of the remineralized DOC in the deep sea is LMW, despite the expected recalcitrance of LMW material (Benner and Amon, 2015). Further, given that LMW material makes up the majority of deep ocean DOC, this result and the prior observation of a significant concentration gradient requires that some portion of LMW be removed on the time scale of deep ocean circulation. When considered relative to the DOC concentration of the HMW UDOM, LMW SPE-DOC, and non-retained fractions individually, the basin offsets correspond to an approximately 30% decrease in DOC in each fraction, apparently suggesting that all three pools are removed at generally similar rates despite the expected differences in reactivity. However, these basin offsets can only show the net change in DOC concentration and cannot differentiate removal from processes that might add material to the deep ocean DOC pool such as dissolution of particles, chemoautotrophy, or hydrothermal sources (e.g., Smith et al., 1992; Ingalls et al., 2006; McCarthy et al., 2010). If there were additions to an individual pool, the apparent utilization of that pool from concentration measurements could represent an underestimation of the actual removed material. Therefore, offsets in properties of each fraction between basins other than concentration must be used in order to deconvolute the influence of additions to the DOC pool from the removal of material.

521 The bulk $\Delta^{14}C$ of DOC represents an average of a heterogeneous pool of material.
522 Despite this, barring any changes to the concentration or distribution of this material, the
523 average $\Delta^{14}C$ of the total DOC pool will change as a function of time. However, because of the
524 removal and potential additions of material with unique radiocarbon content during deep ocean
525 circulation, aging of the total DOC pool cannot be differentiated from these processes. Despite
526 this removal, and potential addition, of DOC during ocean circulation, the radiocarbon age of
527 total DOC is largely conserved. A number of studies have shown that the $\Delta^{14}C$ value of DOC
528 tracks the $\Delta^{14}C$ value of DIC and is consistent with the timescales of water -mass transit times
529 (e.g., Bercovici et al., 2018a; Druffel et al., 2019). Within our separate fractions we hypothesize
530 that changes in $\Delta^{14}C$ that differ from that of total DOC can be interpreted as changes in the age
531 distribution of the pool caused by the removal or addition of DOC. An age offset less than that of
532 the total DOC pool would require fresh inputs of younger material during deep circulation,
533 whereas an age offset greater than total DOC would require the selective removal of younger,
534 more labile material.
535 There are significant $\Delta^{14}C$ offsets ($p < 0.01$) between the deep waters (2500 m) of the
536 Central North Atlantic and NCP in total DOC and in both HMW and LMW DOC fractions (Fig.
537 6b). The average $\Delta^{14}C$ offset at 2500 m is 150 ± 10 ‰ in total DOC, 90 ± 25 ‰ for HMW UDOC,
538 and 140 ± 35 ‰ for the LMW SPE-DOC fraction; representing 2300 ± 200, 1100 ± 200, and
539 2200 ± 500 years respectively (Supplemental Fig. 5). Total DOC, LMW SPE-DOC, and the non-
540 retained DOC all have equivalent age offsets. Combined with the observed concentration
541 offsets discussed above, showing that LMW DOC material is being removed during ocean
542 circulation, this suggests that the removal is non-selective relative to ^{14}C age and there is no
543 significant preferential utilization of younger DOC.
544 In contrast, the apparent age offset of HMW UDOC is substantially less than that of total
545 DOC. We hypothesize that this represents an input of fresh HMW DOC to the deep ocean
546 during circulation and demonstrates that the 30% decrease in HMW DOC concentration
547 between basins is in fact an underestimation of the actual HMW DOC removal, consistent with
548 the higher expected lability of this pool relative to LMW DOC. The $\Delta^{14}C$ value of the “removed”
549 DOC, calculated by mass balance, is 87 ± 166 ‰ for the total DOC pool. It is unreasonable that
550 the DOC removed between the deep North Central Atlantic and the NCP would have a
551 radiocarbon age above modern (Beaupré et al., 2009), and further demonstrates that removal or
552 utilization of DOC is not the only process involved, and there are likely additions of fresher
553 material. The $\Delta^{14}C$ value of removed HMW UDOC is -79 ± 157 ‰ that, as stated above, makes
554 up ~30% of the HMW DOC pool at 2500 m. This value is indistinguishable from the “removed”

555 total DOC and is similarly unlikely, therefore requiring some addition of fresh material.
556 Combined with the other results, the addition of fresher material to the HMW pool likely explains
557 the basin age offsets for both total and HMW DOC. In contrast, the $\Delta^{14}C$ value of removed LMW
558 DOC is -132 ± 125 ‰, consistent with the old LMW material that appears to be utilized during
559 ocean circulation.

560 Despite the suggestion of non-selective removal of LMW DOC from $\Delta^{14}C$ offsets, the
561 observed offsets in C/N ratios in the deep ocean are consistent with selective utilization of more
562 labile LMW material. In both the total DOC pool and in the LMW fraction there is an increase in
563 the C/N ratio between the Central North Atlantic and NCP (Total DOC offset = 7 ± 4; LMW offset
564 = 4 ± 2.5). This increase demonstrates that there is a preferential removal of N-containing
565 material, consistent with expectations for the removal of fresher, less degraded material (Benner
566 and Amon, 2015). In contrast, the lack of any corresponding offset in the HMW DOC fraction
567 suggests that there is either no selectivity in degradation or utilization of HMW material, or as
568 suggested from the ^{14}C age offsets between basins, that there is a relatively constant input of
569 new, young, low C/N material to the HMW DOC pool.

570 While there is clear removal of LMW DOC during ocean circulation, difference spectra
571 indicate that there is essentially no change in the functional composition of this material during
572 deep ocean circulation. This suggests that, in contrast to HMW DOM, the removal of LMW DOC
573 is completely non-selective. This NMR-based conclusion corresponds to the traditional view of a
574 refractory “background” pool, however at the same time is inconsistent with the $\Delta^{14}C$ and C/N
575 offsets in LMW SPE-DOC between ocean basins. There are several possible explanations for
576 this apparent contrast. First, it is possible that the selective utilization of specific compound
577 types cannot be determined at the functional group level of resolution provided by these NMR
578 measurements. However, the changes in $\Delta^{14}C$ of this material combined with the functional
579 similarity of LMW SPE-DOC material in the surface and deep ocean, despite the large age
580 gradient with depth, more likely demonstrates that freshly produced LMW DOC and older LMW
581 material that survives mixing into the deep ocean both represent a similar mixture of compound
582 structures containing the same dominant functional groups. This suggests that the pool of
583 CRAM molecules is a heterogeneous mixture of compounds with different cycling rates but
584 generally similar structures. Second, the increase in C/N ratio between basins, implying a
585 selective loss of N-containing compounds, potentially demonstrates that N-containing material
586 within the LMW pool has a generally similar functional composition as the bulk material. In other
587 words, this suggests that there is a substantial amount of N-containing CRAM molecules in the
588 deep ocean.

In contrast, while there is no change in the elemental ratios of HMW UDOM, solid-state NMR difference spectra indicate differences in the functional composition of this material in the deep ocean between the Atlantic and Pacific (Fig. 7c). In the HMW fraction the primary difference between spectra corresponds to a higher relative proportion of alkoxy and carboxyl C in the deep waters of the Pacific. The apparent increase in alkoxy C during deep water transit is the opposite of the trend observed between surface and deep waters in both basins and suggests that rather than the removal of a more reactive carbohydrate-like fraction during deep ocean circulation, there is some amount of carbohydrate-like material added to the deep ocean HMW DOC pool. We note that the difference spectra also reveal considerably more alkoxy C in the surface waters of the NCP than the surface waters of the Central North Atlantic (Fig. 7c). Since surface composition is linked to more rapid local processes, this difference in the surface between basins likely represents a difference in overall biogeochemistry at these two sites. Since highly oligotrophic, microbial loop dominated regions generally correspond with both elevated DOC concentration and C/N ratio, this offset in bulk composition is likely due to the consistently oligotrophic nature of the HOT site (Williams, 1995; Hansell and Carlson, 2001).

5.0 Summary and Conclusions

A combination of ultrafiltration and solid phase extraction was used to specifically isolate HMW and LMW DOC from throughout the water column in both the Central North Atlantic and NCP Subtropical Gyres. The novel LMW fraction collected for this study represents a new and direct approach to investigate the composition and cycling of a large fraction of the DOC pool that dominates the refractory background pool and persists in the ocean for millennial timescales.

Compared to the total DOC pool, or the more commonly studied HMW DOC pool, the LMW SPE-DOC fraction isolated for this study is older, with depleted $\delta^{13}C$ values, higher C/N ratios, and a composition dominated by alkyl and carboxyl functional groups. NMR analyses of LMW DOC components demonstrate that the functional composition is essentially identical throughout the water column and in both ocean basins (Fig. 4b), suggesting a uniform background DOC pool. The specific distribution of functional groups is remarkably similar to the CRAM family of structures that has been proposed as a major component of refractory marine DOC. This is consistent with the slower cycling rates suggested by the considerably older average ^{14}C ages of the LMW SPE-DOC fraction.

Despite the suggestion from structural composition data that LMW DOC is a homogeneous refractory background pool, there is also clear evidence for active cycling within the LMW pool. Depth changes in elemental ratios and isotopic values of LMW SPE-DOC suggest that there is labile, C-rich material that dominates the surface LMW DOC pool but is remineralized on timescales shorter than ocean circulation. Further, the clear shifts in LMW SPE-DOC age with depth suggest that it spans a range of reactivities and cycling rates. There is also clear removal of LMW DOC in the deep ocean during overturning circulation accompanied by changes that are consistent with the preferential utilization of a less refractory LMW component. NMR results also suggest the presence of essentially indistinguishable CRAM material within the HMW fraction, indicating that CRAM spans a wide range of molecular sizes and is therefore not exclusively derived from the microbial degradation of labile HMW material.

Relative to the LMW SPE-DOC fraction, the HMW DOC isolated for this study has younger ^{14}C ages, enriched $\delta^{13}C$ values, lower C/N ratios and a dominant carbohydrate like composition. Basin concentration offsets show removal of HMW DOC during overturning circulation, however ^{14}C age offsets are less than can be accounted for based solely on aging, suggesting the addition of younger HMW material to the deep ocean. This is consistent with NMR data that demonstrate an increase in carbohydrate-like material in the deep ocean during deep ocean circulation. We hypothesize this represents a bulk structural signature resulting from the dissolution of sinking particles, with fresh carbohydrate material being added to the relatively small HMW DOC pool that survives in the deep ocean. This observation is consistent with previous ^{14}C data suggesting a likely source of neutral sugars to the deep ocean from rapidly sinking particles (Repeta and Aluwihare, 2006; Walker et al., 2016a). Overall, our data suggest that particle inputs to the deep ocean are likely important in maintaining deep ocean HMW DOC concentrations.

These first direct analyses of the LMW DOC pool and comparison to the more commonly investigated HMW DOC pool provided data consistent with many basic assumptions about both the differential cycling of different MW pools and the presence of a refractory background pool dominated by CRAM like molecular structures. However, despite a generally invariable functional composition, LMW DOC is likely a more dynamic pool than was previously recognized, with properties implying a diverse, wide ranging family of CRAM like molecules in terms of molecular size, N-content and relative reactivity. Our data also point to an unexpected influence of surface particle flux in both maintaining deep ocean HMW DOC concentrations and shaping its molecular composition. Future work should focus on the specific molecular structures of CRAM like material across a range of DOC molecular sizes and what properties

potentially govern the differences in relative reactivity of the different structurally related compounds.

6.0 Figure and Table Captions

Figure 1. Total DOC concentration and amount of C recovered with a combined UF/SPE approach. Depth profiles of (a) total DOC concentration, (b) DOC isolated by ultrafiltration and (c) solid phase extraction, and (d) non-retained DOC. Points connected by solid lines represent samples collected in the North Central Pacific (HOT), and dotted lines represent samples collected in the Central North Atlantic (BATS). Points represent the error weighted average of values from 2 repeat cruise samplings in May and August, and error bars represent the standard error.

Figure 2. Radiocarbon content ($\Delta^{14}C$) of total DOC and C recovered with a combined UF/SPE approach. Depth profiles of (a) total DOC, (b) HMW UDOC, (c) LMW SPE-DOC, and (d) the non-retained material (calculated by difference). Points connected by solid lines represent samples collected in the North Pacific Subtropical Gyre (HOT), and dotted lines represent samples collected in the Central North Atlantic (BATS). Points represent the error weighted average of values from 2 repeat cruise samplings in May and August, and error bars represent the standard error. The uncertainty of the non-retained fraction represents the propagated error associated with instrumental uncertainty of both the DOC concentrations and $\Delta^{14}C$ values. Samples for total DOC ^{14}C analyses were only collected at BATS during the May sampling cruise, the error bars for these values represent the instrument uncertainty of ± 5 ‰.

Figure 3. Carbon to nitrogen elemental ratios $(C/N)_a$ and stable C isotopes ($\delta^{13}C$) of total DOM and DOM recovered with a combined UF/SPE approach. Depth profiles of (a and e) total DOM, (b and f) HMW UDOM, (c and g) LMW SPE-DOM and (d and h) the non-retained material (calculated by difference). Points connected by solid lines represent samples collected in the North Central Pacific (HOT), and dotted lines represent samples collected in the Central North Atlantic (BATS). Points represent the error weighted average of n=3 measurements from material collected on each of 2 repeat cruise samplings in May and August, and error bars represent the standard error. The uncertainty of the C/N ratio and $\delta^{13}C$ of the non-retained fraction represents the propagated error associated with instrumental uncertainty of isotopic

values and/or DOC/DON concentrations. Samples for total DOC ^{13}C analyses were only collected at BATS during the May sampling cruise, the error bars for these values represent the instrument uncertainty of ± 0.2 ‰.

Figure 4. Solid-state 13C NMR spectra of HMW UDOC and LMW SPE-DOC. (a) spectra of HMW UDOC collected in the surface (purple) and deep ocean (2500m; light blue) from the Central North Atlantic (BATS; dashed lines) and North Central Pacific (HOT; solid lines). (b) spectra of LMW SPE-DOC collected in the surface (dark red) and deep ocean (2500m; orange) from BATS (dashed lines) and HOT (solid lines). Spectral assignments are as follows: ketone, aldehyde, quinone (220-191 ppm); COO, NC=O (191-164 ppm); aromatic C-O (164-150 ppm); aromatics (150-117 ppm); OCO (94-60 ppm); OC (94-60 ppm); OCH3, NCH (60-45 ppm); CCH2C, CCHC (45-30 ppm); CCH2C, CCH3 (30-0 ppm). Regions have been combined (as in Koprivnjak et al., 2009), resulting in four generalized groupings: carboxyl C (220-164 ppm), aromatic C (164-117 ppm), alkoxy C (117-60 ppm), and alkyl C (60-0 ppm). Spectra showing all functional group assignments are presented in Supplemental Figure 2.

Figure 5. Offsets between the surface and 2500 m of (a) the concentration (ΔDOC) and (b) radiocarbon content ($\Delta\Delta^{14}C$) of total DOC and material recovered with a combined UF/SPE approach. Solid bars represent the surface versus deep offset in the NPSG and striped bars represent the surface versus deep offset in the Central North Atlantic. Values represent the offsets between error weighted averages of values from 2 repeat cruise samplings in May and August, and error bars represent the propagated standard deviation of both sampling seasons and both depths. The uncertainty of the non-retained fraction represents the propagated error associated with instrumental uncertainty of the DOC concentrations and isotopic values.

Figure 6. Basin offsets between the Central North Atlantic (BATS) and North Central Pacific (HOT) of (a) the concentration (ΔDOC) and (b) radiocarbon values ($\Delta\Delta^{14}C$) of total DOC and material recovered with a combined UF/SPE approach at 2500 m. Values represent the offsets between error weighted averages of values from 2 repeat cruise samplings in May and August, and error bars represent the propagated standard deviation of both sampling seasons and both basins.

Figure 7. Area normalized solid-state ^{13}C NMR difference spectra from HMW UDOC and LMW SPE-DOC. (a) difference between surface and deep (2500 m) HMW UDOC material in the

721 North Central Pacific (HOT; purple) and Central North Atlantic (BATS; light blue). (b) difference
722 between surface and deep (2500 m) LMW SPE-DOC material at HOT (red) and BATS (orange).
723 (c) difference between HMW UDOC material collected at HOT and BATS from surface (purple)
724 and deep ocean (2500 m; light blue). (d) difference between LMW UDOC material collected at
725 HOT and BATS from surface (red) and deep ocean (2500 m; orange). Values above the
726 baseline demonstrate the removal of material with depth or between basins (from surface to
727 deep or BATS to HOT) and values below the baseline demonstrate the addition of material with
728 depth or between basins (from surface to deep or BATS to HOT).
729
730 Table 1. Properties of total DOM from which MW fractions were isolated including concentration,
731 C/N ratio, and carbon isotopes ($\delta^{13}C$, $\Delta^{14}C$)
732
733 Table 2. Isolation parameters and properties of LMW SPE-DOM and HMW UDOM fractions
734 including recovery efficiency, C/N ratio, and carbon isotopes ($\delta^{13}C$, $\Delta^{14}C$). Stable isotopic ($\delta^{13}C$)
735 values and C/N ratios represent the average of n=3 measurements of each sample and errors
736 represent the standard deviation. Radiocarbon ($\Delta^{14}C$) errors represent the instrument
737 uncertainty.

738

739 **7.0 Acknowledgements, Samples, and Data**

740 The authors would foremost like to thank the captains and crews of the UNOLS vessels R/V Kilo
741 Moana and R/V Atlantic Explorer whose effort allowed for the collection of this novel sample set.
742 Additional thanks to Amy Bour, Jessie Zupcic-Moore, Danielle Creeley, Yasu Yamaguchi,
743 Danielle Glynn, Hope Ianiri, Yuan Shen, and Ron Benner for assistance with sample collection
744 and processing, Colin Carney and Dyke Andreasen of UCSC-SIL for assisting with EA-IRMS
745 analysis, Alexandra Hedgpeth and Paula Zermeno of LLNL-CAMS for assistance with AMS
746 sample preparation, and Kimber Moreland for assistance with NMR spectral integration and
747 processing.

748 All data aside from NMR spectral data are presented in tables within the main text and
749 supplemental materials of this manuscript and is publicly available in the BCO-DMO data
750 repository. Data archiving of NMR spectra and integrations is underway in the BCO-DMO data

repository. Pending archiving completion, the data are available as Supporting Information accompanying this submission.

This work was primarily supported by a grant from NSF Chemical Oceanography (Award # 1358041) and supported in part by funding from the Canada Research Chair program to B.D.W. Total DOC ^{14}C analysis was performed under a UCI Keck Carbon Cycle AMS Lab postdoctoral scholarship to B.D.W. A portion of this work was performed under the auspices of the U.S. Department of Energy by Lawrence Livermore National Laboratory under Contract DE-AC52-07NA27344.

8.0 References

Amon, R. M. W., Benner, R., 1996. Bacterial utilization of different size classes of dissolved organic matter. Limnology and Oceanography 41, 41–51.

Amon, R. M. W., Benner, R., 1994. Rapid cycling of high-molecular-weight dissolved organic matter in the ocean. Nature 369, 549–552.

Bauer, J. E., Williams, P. M., Druffel, E. R. M., 1992. C-14 activity of dissolved organic carbon fractions in the north-central Pacific and Sargasso Sea. Nature 357, 667–670.

Beaupré, S. R., Druffel, E. R. M., 2009. Constraining the propagation of bomb-radiocarbon through the dissolved organic carbon (DOC) pool in the northeast Pacific Ocean. Deep-Sea Research Part I – Oceanography Research Papers 56, 1717–1726.

Beaupré, S. R., Druffel, E. R. M., Griffin, S., 2007. A low-blank photochemical extraction system for concentration and isotopic analyses of marine dissolved organic carbon. Limnology and Oceanorgaphy Methods 5, 174–184.

Benner, R., Amon, R. M. W., 2015. The size-reactivity continuum of major bioelements in the ocean. Annual Reviews of Marine Science 7, 185–205.

Benner, R., Biddanda, B., Black, B., McCarthy, M. D., 1997. Abundance, size distribution, and stable carbon and nitrogen isotopic compositions of marine organic matter isolated by tangential-flow ultrafiltration. Marine Chemistry 57, 243–263.

Benner R., Bodungen, V. B., Farrington, J., Hedges, J., Lee, C., Mantoura, F., Suzuki, Y., Williams, P. M., 1993. Measurement of dissolved organic carbon and nitrogen in natural waters: Workshop report. Marine Chemistry 41, 5–10.

Benner, R., Pakulski, J. D., McCarthy, M. D., Hedges, J. I., Hatcher, P. G., 1992. Bulk chemical characteristics of dissolved organic matter in the ocean. Science 255, 1561–1564.

Bercovici, S. K., McNichol, A. P., Xu, L. and Hansell, D. A., 2018a. Radiocarbon Content of Dissolved Organic Carbon in the South Indian Ocean. Geophysical Research Letters 45, 872–879.

Bercovici, S. K., Koch, B. P., Lechtenfeld, O. J., Mccallister, S. L., Schmitt-Kopplin, P., Hansell, D. A., 2018b. Aging and Molecular Changes of Dissolved Organic Matter Between Two Deep Oceanic End-Members. Global Biogeochemical Cycles 32, 1449-1456.

Broek, T. A. B., Bour, A. L., Ianiri, H. L., Guilderson, T. P., McCarthy, M. D., 2019. Amino acid enantiomers in old and young dissolved organic matter: implications for a microbial nitrogen pump. Geochimica et Cosmochimica Acta 247, 207–219.

Broek, T. A. B., Walker, B. D., Guilderson, T. P., McCarthy, M. D., 2017. Coupled ultrafiltration and solid phase extraction approach for the targeted study of semi-labile high molecular weight and refractory low molecular weight dissolved organic matter. Marine Chemistry 194, 146-157.

Carlson, C. A., Hansell, D. A., 2014. DOM sources, sinks, reactivity, and budgets, in: Hansel, D. A., Carlson, C. A. (Eds.), The Biogeochemistry of Marine Dissolved Organic Matter. Academic Press, pp. 65–126.

Coppola, A. I., Walker, B. D., Druffel, E. R. M., 2015. Solid phase extraction method for the study of black carbon cycling in dissolved organic carbon using radiocarbon. Marine Chemistry 177, 697–705.

DeVries, T., Primeau, F., 2011. Dynamically and Observationally Constrained Estimates of Water-Mass Distributions and Ages in the Global Ocean. Journal of Physical Oceanography 41, 2381–2401.

Druffel, E. R. M., Griffin, S., Wang, N., Garcia, N. G., McNichol, A. P., Key, R. M., Walker, B. D., 2019. Dissolved Organic Radiocarbon in the Central Pacific Ocean. Geophysical Research letters 46, 5396–5403.

Druffel, E. R. M., Griffin, S., Coppola, A. I., Walker, B. D., 2016. Radiocarbon in dissolved organic carbon of the Atlantic Ocean. Geophysical Research Letters 43, 5279–5286.

Druffel, E. R. M., Griffin, S., Walker, B. D., Coppola, A. I., Glynn, D. S., 2013. Total uncertainty of radiocarbon measurements of marine dissolved organic carbon and methodological recommendations. Radiocarbon 55, 1135–1141.

Druffel, E. R. M., Williams, P. M., Bauer, J. E., Ertel, J. R., 1992. Cycling of dissolved and particulate organic-matter in the open ocean. Journal of Geophysical Research 97, 15639–15659.

Flerus, R., Lechtenfeld, O. J., Koch, B. P., McCallister, S. L., Schmitt-Kopplin, P., Benner, R., Kaiser, K. and Kattner, G., 2012. A molecular perspective on the ageing of marine dissolved organic matter. Biogeosciences 9, 1935–1955.

Guo, L., Santschi, P. H., Cifuentes, L. A., Trumbore, S. E., Southon, J., 1996. Cycling of high-molecular-weight dissolved organic matter in the Middle Atlantic Bight as revealed by carbon isotopic (^{13}C and ^{14}C) signatures. Limnology and Oceanography 41, 1242–1252.

Hansell, D. A., 2013a. Recalcitrant dissolved organic carbon fractions. Annual Review of Marine Science 5, 421–445.

Hansell, D. A., Carlson, C. A., 2013b. Localized refractory dissolved organic carbon sinks in the deep ocean. Global Biogeochemical Cycles 27, 705–710.

Hansman, R.L., Dittmar, T., Herndl, G. J., 2015. Conservation of dissolved organic matter molecular composition during mixing of the deep water masses of the northeast Atlantic Ocean. Marine Chemistry 177, 288–297.

Hayes, J. M., 2001. Fractionation of carbon and hydrogen isotopes in biosynthetic processes. Reviews of Mineral Geochemistry 43, 225–277.

Hertkorn, N., Benner, R., Frommberger, M., Schmitt-Kopplin, P., Witt, M., Kaiser, K., Kettrup, A., Hedges, J. I., 2006. Characterization of a major refractory component of marine dissolved organic matter. Geochimica et Cosmochimica Acta 70, 2990–3010.

Hwang, J., 2003. Lipid-like material as the source of the uncharacterized organic carbon in the ocean? Science 299, 881–884.

Ingalls, A. E., Shah, S. R., Hansman, R. L., Aluwihare, L. I., Santos, G. M., Druffel, E. R. M., Pearson, A., 2006. Quantifying archaeal community autotrophy in the mesopelagic ocean using natural radiocarbon. Proceedings of the National Academy of Sciences 103, 6442-6447.

Kaiser, K., Benner, R., 2009. Biochemical composition and size distribution of organic matter at the Pacific and Atlantic time-series stations. Marine Chemistry 113, 63–77.

Kaiser, K., Benner, R., 2008. Major bacterial contribution to the ocean reservoir of detrital organic carbon and nitrogen. Limnology and Oceanography 53, 99–112.

Koprivnjak, J. F., Pfromm, P. H., Ingall, E., Vetter, T. A., Schmitt-Kopplin, P., Hertkorn, N., Frommberger, M., Knicker, H., Perdue, E. M., (2009) Chemical and spectroscopic characterization of marine dissolved organic matter isolated using coupled reverse osmosis–electrodialysis. Geochimica et Cosmochimica Acta 73, 4215–4231.

Lechtenfeld, O. J., Kattner, G. and Flerus, R., 2014. Molecular transformation and degradation of refractory dissolved organic matter in the Atlantic and Southern Ocean. Geochimica et Cosmochimica Acta 126, 321–337.

Li, S., Zhang, Y., Hong, M., 2010. 3D ^{13}C–^{13}C–^{13}C correlation NMR for de novo distance

883 determination of solid proteins and application to a human A-defensin. Journal of Magnetic
884 Resonance 202, 203–210.
885
886 Mao, J., Kong, X., Schmidt-Rohr, K., Pignatello, J. J., Perdue E. M., 2012. Advanced solid-state
887 NMR characterization of marine dissolved organic matter isolated using the coupled reverse
888 osmosis/electrodialysis method. Environmental Science and Technology 46, 5806–5814.
889
890 McCarthy, M. D., Hedgesm J. I., Benner, R., 1996. Major biochemical composition of dissolved
891 high molecular weight organic matter in seawater. Marine Chemistry 55, 281–297.
892
893 McCarthy, M. D., Hedges, J. I. and Benner, R., 1993. The chemical composition of dissolved
894 organic matter in seawater. Chemical Geology 107, 503–507.
895
896 Repeta, D. J., Aluwihare, L. I., 2006. Radiocarbon analysis of neutral sugars in high-molecular-
897 weight dissolved organic carbon: Implications for organic carbon cycling. Limnology and
898 Oceanography 51, 1045–1053.
899
900 Sannigrahi, P., Ingall, E. D., Benner, R., 2005. Cycling of dissolved and particulate organic
901 matter at station aloha: insights from ^{13}C NMR spectroscopy coupled with elemental, isotopic
902 and molecular analyses. Deep-Sea Research Part I 52, 1429–1444.
903
904 Santos, G. M., Southon, J. R., Griffin, S., Druffel E. R. M., Beaupré S. R., 2007. Ultra small-
905 mass AMS ^{14}C sample preparation and analyses at KCCAMS/UCI Facility. Nuclear Instruments
906 and Methods in Physics Research Section B: Beam Interactions with Materials and Atoms 259,
907 293–302.
908
909 Shen and Benner, 2019. Molecular Properties are a primary control on the microbial utilization
910 of dissolved organic matter in the ocean. Limnology and Oceanography X, X-X.
911
912 Smith, D. C., Simon, M., Alldredge, A. L., Azam, F., 1992. Intense hydrolytic enzyme activity on
913 marine aggregates and implications for rapid particle dissolution. Nature 359, 139–142.
914
915 Stuiver, M., Polach, H. A., 1977. Discussion reporting of ^{14}C data. Radiocarbon 19, 355–363.
916

Taylor, J. R., 1997. *An introduction to Error Analysis (second edition)*. Sausalito, CA: University Science Books.

Vetter, T. A., Perdue, E. M., Ingall, E., Koprivnjak, J. F., Pfromm, P. H., 2007. Combining reverse osmosis and electrodialysis for more complete recovery of dissolved organic matter from seawater. Separation and Purification Technology 56, 383–387.

Vetter, T. A., Perdue, E. M., Ingall, E., Koprivnjak, J. F., Pfromm, P. H., 2007. Combining reverse osmosis and electrodialysis for more complete recovery of dissolved organic matter from seawater. Separation and Purification Technology 56, 383–387.

Vogel, J. S., Southon, J. R., Nelson, D. E., Brown, T. A., 1984. Performance of catalytically condensed carbon for use in accelerator mass-spectrometry. Nuclear Instrumental Methods in Physical Research Section B: Beam Interactions with Materials and Atoms 5, 289–293.

Walker, B. D., Beaupré, S. R., Guilderson, T. P., Druffel, E. R. M., McCarthy, M. D., 2011. Large-volume ultrafiltration for the study of radiocarbon signatures and size vs. age relationships in marine dissolved organic matter. Geochimica et Cosmochimica Acta 75, 5187–5202.

Walker, B. D., Beaupré, S. R., Guilderson, T. P., McCarthy, M. D., Druffel, E.R.M., 2016a. Pacific carbon cycling constrained by organic matter size, age and composition relationships. Nature Geoscience 9, 888-891.

Walker, B. D., Griffin, S., Druffel, E., 2016b. Effect of acidified versus frozen storage on marine dissolved organic carbon concentration and isotopic composition. Radiocarbon 59, 843-857.

Walker, B. D., Primeau, F. W., Beaupré, S. R., Guilderson, T. P., Druffel, E .R. M., McCarthy, M.D., 2016c. Linked changes in marine dissolved organic carbon molecular size and radiocarbon age. Geophysical Research Letters 43, 10,385–10,393.

Walker, B. D., Guilderson, T. P., Okimura, K. M., 2014. Radiocarbon signatures and size–age–composition relationships of major organic matter pools within a unique California upwelling system. Geochimica et Cosmochimica Acta 126, 1–17.

Williams, P. J. leB., 1995. Evidence for the seasonal accumulation of carbon-rich dissolved organic material, its scale in comparison with changes in particulate material and the consequential effect on net C/N assimilation ratios. Marine Chemistry 51, 17-29.

Williams, P. M., Druffel, E. R. M., 1987. Radiocarbon in dissolved organic matter in the central North Pacific Ocean. Nature 330, 246–248.

Zigah, P. K., McNichol, A. P., Xu, L., Johnson, C., Santinelli, C., Karl, D. M., Repeta D. J., 2017. Allochthonous sources and dynamic cycling of ocean dissolved organic carbon revealed by carbon isotopes. Geophysical Research Letters 49, 4421–9.

Ziolkowski, L. A., Druffel, E. R. M., 2010. Aged black carbon identified in marine dissolved organic carbon. Geophysical Research Letters 37, L16601.

Figure 1.

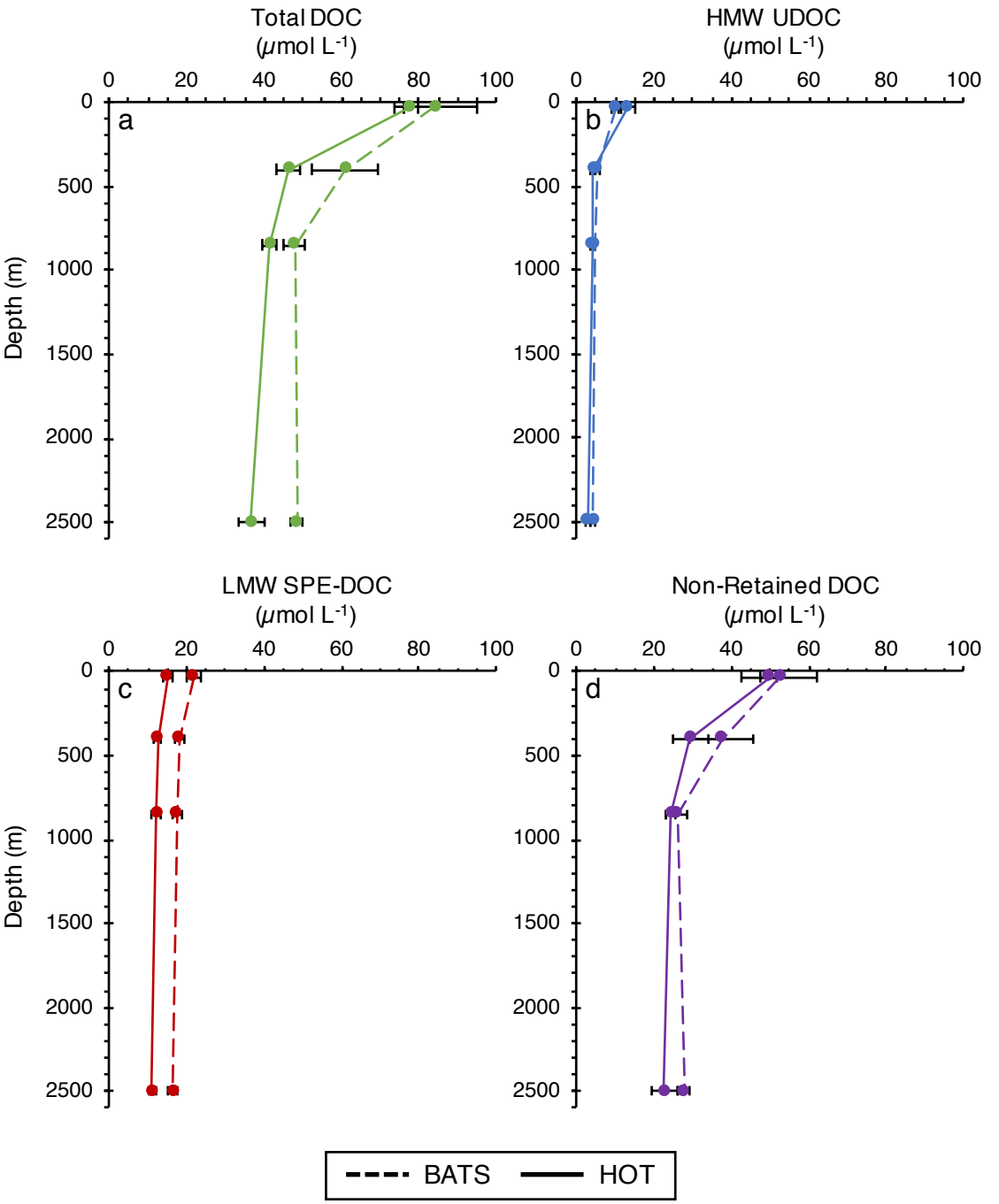
Total DOC
(μmol L-1)
HMW UDOC
(μmol L-1)
LMW SPE-DOC
(μmol L-1)
Non-Retained DOC
(μmol L-1)
a
b
c
d
Depth (m)
0
20
40
60
80
100
500
1000
1500
2000
2500
BATS
HOT

Figure 2.

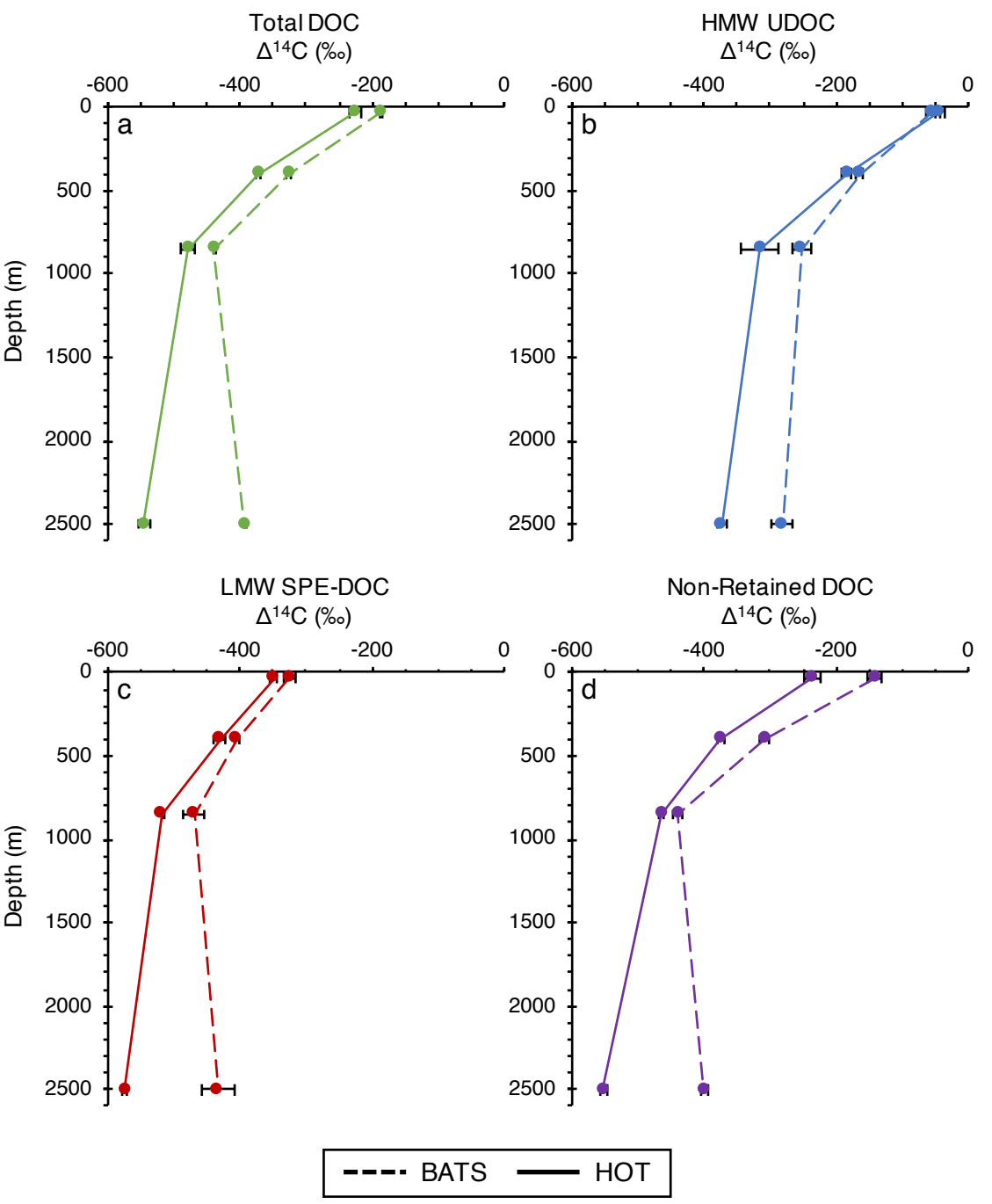
Total DOC
Δ14C (‰)
HMW UDOC
Δ14C (‰)
LMW SPE-DOC
Δ14C (‰)
Non-Retained DOC
Δ14C (‰)
-600
-400
-200
0
Depth (m)
0
500
1000
1500
2000
2500
a
b
c
d
BATS
HOT

Figure 3.

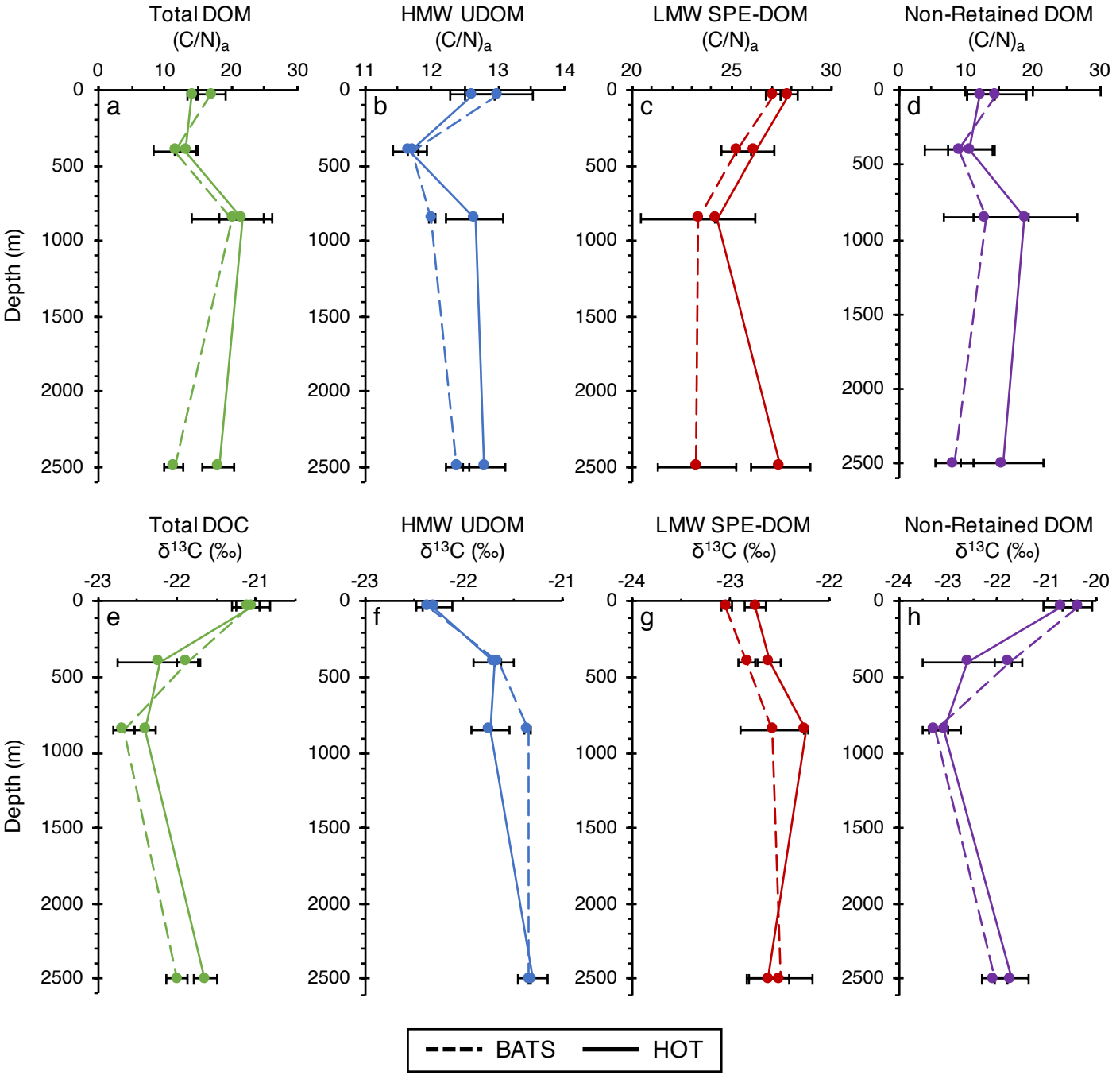
Total DOM
(C/N)a
HMW UDOM
(C/N)a
LMW SPE-DOM
(C/N)a
Non-Retained DOM
(C/N)a
Depth (m)
a
b
c
d
Total DOC
δ13C (‰)
HMW UDOM
δ13C (‰)
LMW SPE-DOM
δ13C (‰)
Non-Retained DOM
δ13C (‰)
e
f
g
h
BATS
HOT

Figure 4.

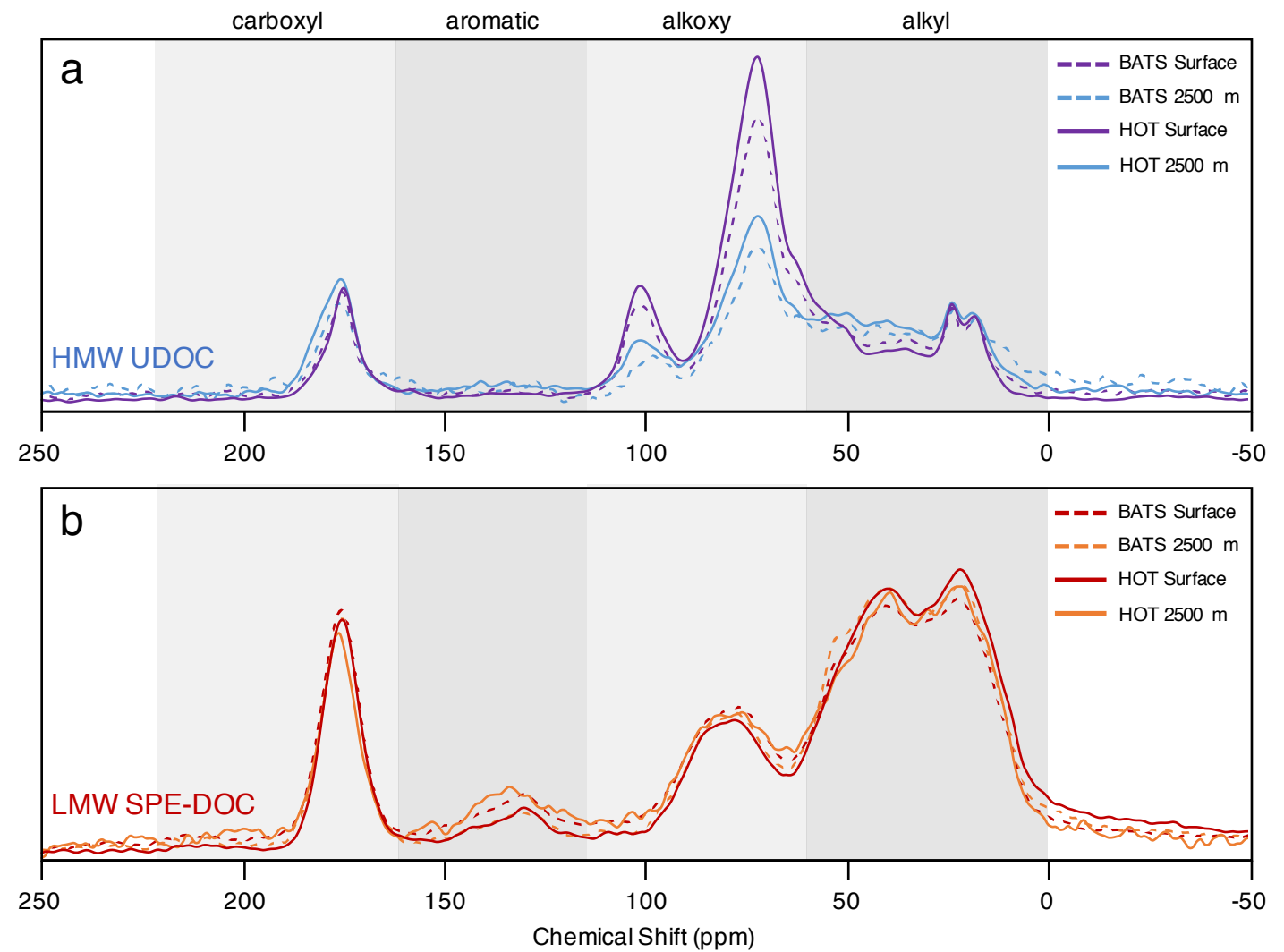
carboxyl
aromatic
alkoxy
alkyl
a
BATS Surface
BATS 2500 m
HOT Surface
HOT 2500 m
HMW UDOC
250
200
150
100
50
0
-50
b
BATS Surface
BATS 2500 m
HOT Surface
HOT 2500 m
LMW SPE-DOC
250
200
150
100
50
0
-50
Chemical Shift (ppm)

Figure 5.

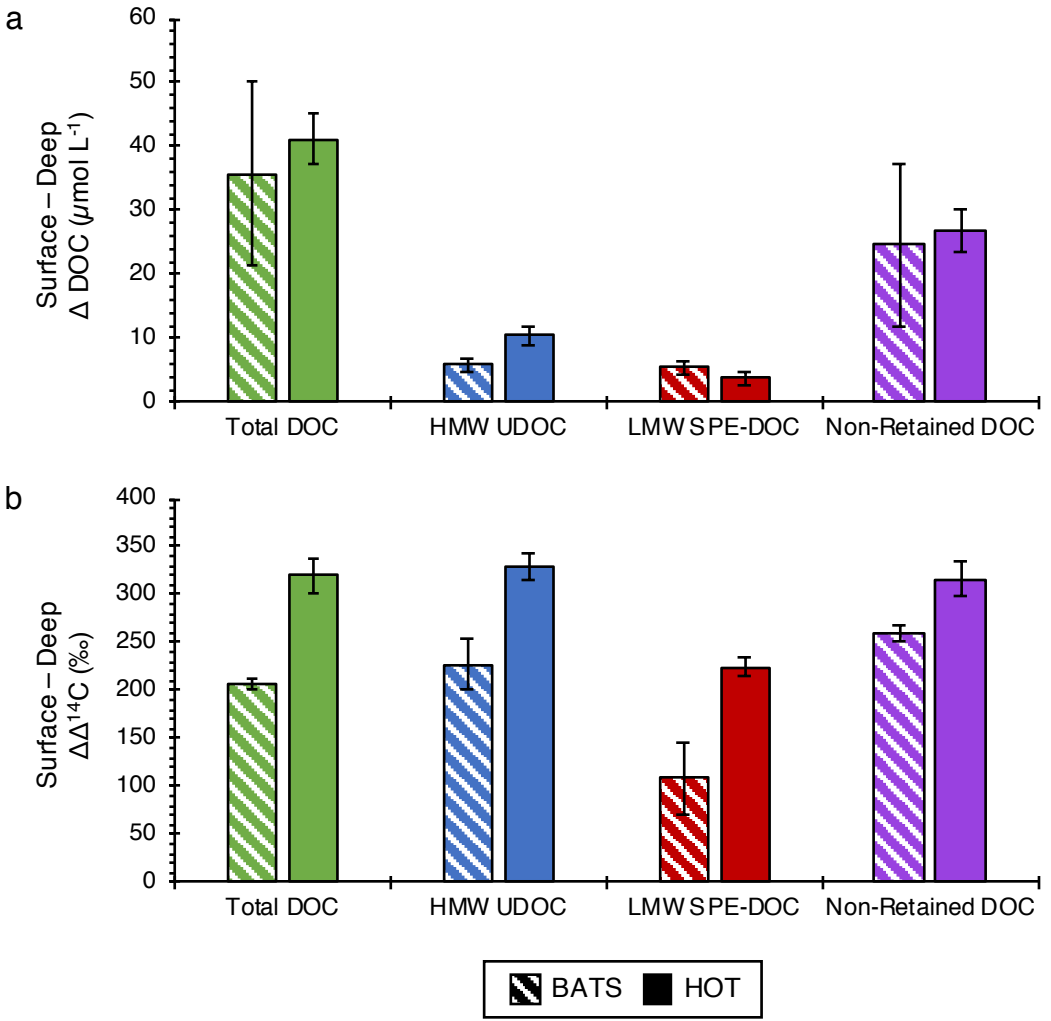
a
Surface – Deep
Δ DOC (μmol L-1)
60
50
40
30
20
10
0
Total DOC
HMW UDOC
LMW SPE-DOC
Non-Retained DOC
b
Surface – Deep
ΔΔ14C (‰)
400
350
300
250
200
150
100
50
0
Total DOC
HMW UDOC
LMW SPE-DOC
Non-Retained DOC
BATS
HOT

Figure 6.

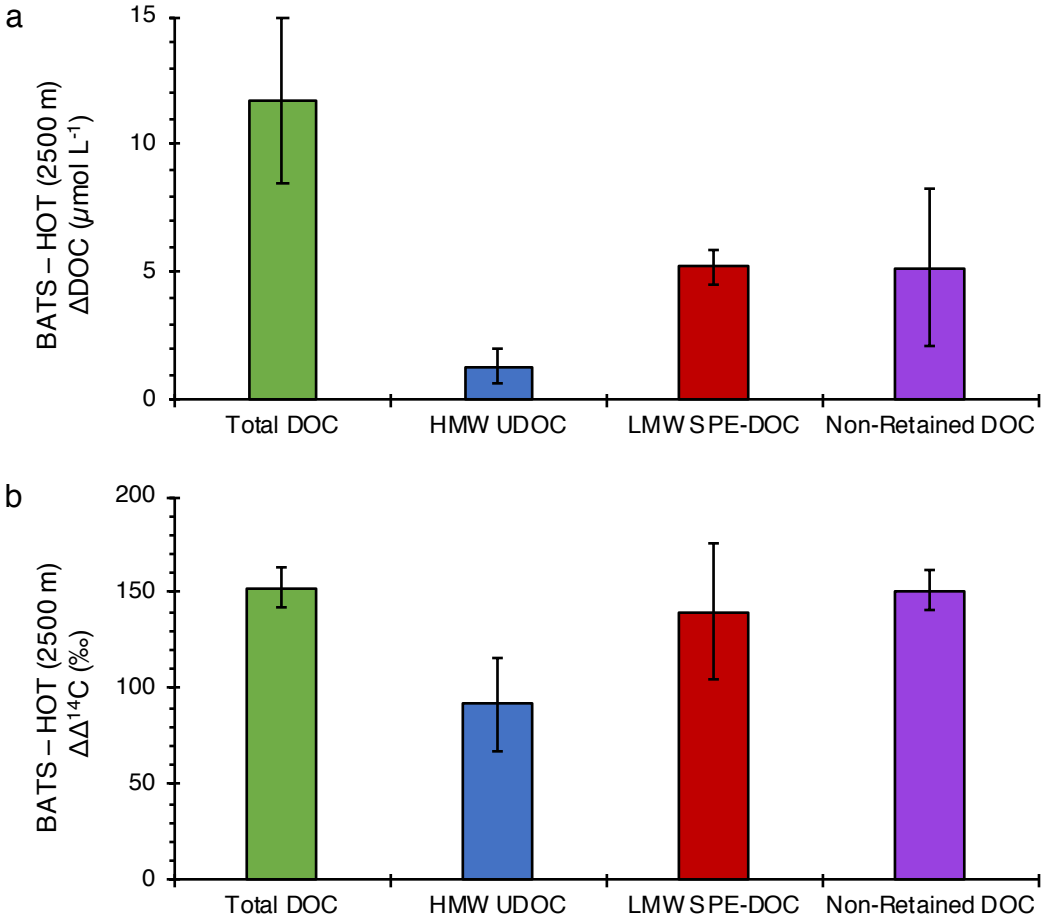
a
BATS – HOT (2500 m)
ΔDOC (μmol L-1)
15
10
5
0
Total DOC
HMW UDOC
LMW SPE-DOC
Non-Retained DOC
b
BATS – HOT (2500 m)
ΔΔ14C (‰)
200
150
100
50
0
Total DOC
HMW UDOC
LMW SPE-DOC
Non-Retained DOC

Figure 7.

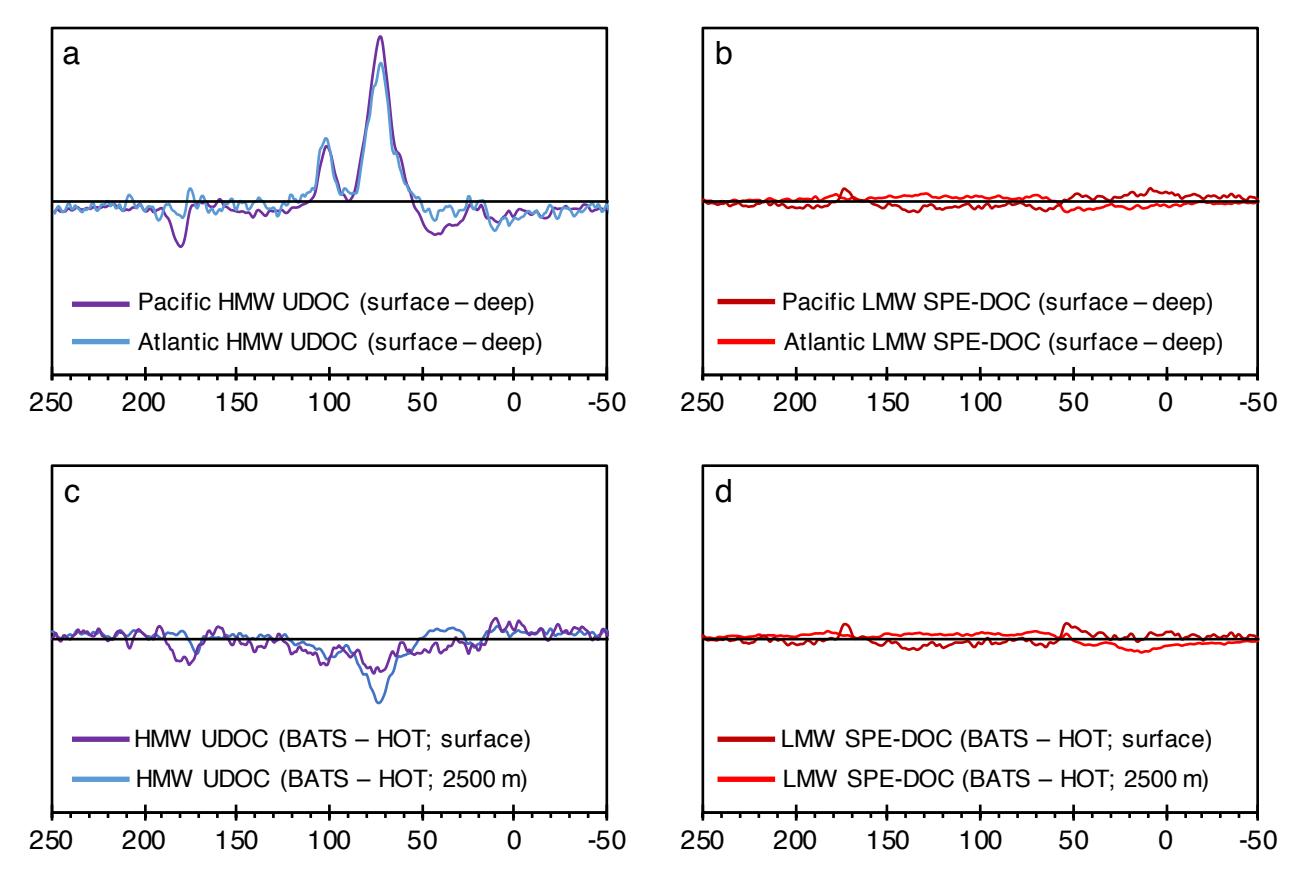
a
Pacific HMW UDOC (surface – deep)
Atlantic HMW UDOC (surface – deep)
250
200
150
100
50
0
-50
b
Pacific LMW SPE-DOC (surface – deep)
Atlantic LMW SPE-DOC (surface – deep)
250
200
150
100
50
0
-50
c
HMW UDOC (BATS – HOT; surface)
HMW UDOC (BATS – HOT; 2500 m)
250
200
150
100
50
0
-50
d
LMW SPE-DOC (BATS – HOT; surface)
LMW SPE-DOC (BATS – HOT; 2500 m)
250
200
150
100
50
0
-50

location	year	month	sample type	depth (m)	[DOC] (μM)	±	C/N	±	UCIAMS #	$\delta^{13}C$ (‰)	±	Fm	±
HOT	2014	August	Total DOM	7.5	79.8	0.6	14.1	1.6	158141	-20.8	0.2	0.7911	0.0026
HOT	2014	August	Total DOM	400	47.2	2.8	13.2	1.7	158145	-22.7	0.2	0.6343	0.0023
HOT	2014	August	Total DOM	850	41.0	1.1	19.7	5.0	158144	-22.4	0.2	0.5375	0.0026
HOT	2014	August	Total DOM	2500	34.8	5.3	17.8	4.8	158143	-21.8	0.2	0.4663	0.0020
HOT	2015	May	Total DOM	7.5	75.9	1.2	14.3	1.8	164612	-21.3	0.2	0.7715	0.0019
HOT	2015	May	Total DOM	400	45.5	7.8	13.1	3.9	164613	-21.7	0.2	0.6308	0.0017
HOT	2015	May	Total DOM	850	41.8	4.6	23.4	6.1	168551	--	--	0.5140	0.0018
HOT	2015	May	Total DOM	2500	38.6	5.3	18.4	4.9	168540	-21.5	0.2	0.4519	0.0022
BATS	2015	August	Total DOM	7.5	94.3	4.9	18.7	3.5	--	--	--	--	--
BATS	2015	August	Total DOM	400	69.0	8.6	14.1	4.8	--	--	--	--	--
BATS	2015	August	Total DOM	850	50.5	1.1	15.2	1.7	--	--	--	--	--
BATS	2015	August	Total DOM	2500	49.7	1.9	11.8	2.8	--	--	--	--	--
BATS	2016	May	Total DOM	7.5	74.1	7.8	15.3	2.6	180280	-21.1	0.2	0.8204	0.0018
BATS	2016	May	Total DOM	400	52.9	1.1	9.2	4.1	180269	-21.9	0.2	0.6793	0.0016
BATS	2016	May	Total DOM	850	45.1	1.6	25.0	12.2	180271	-22.7	0.2	0.5662	0.0016
BATS	2016	May	Total DOM	2500	47.1	1.2	11.0	2.7	180276	-22.0	0.2	0.6129	0.0018

$\Delta^{14}C$ (‰)	±	^{14}C age (ybp)	±
-215.1	2.6	1880	30
-370.6	2.3	3655	30
-466.7	2.6	4985	40
-537.4	2.0	6130	35
-234.5	1.9	2085	25
-374.1	1.7	3700	25
-490.0	1.8	5345	30
-551.6	2.2	6380	40
--	--	--	--
--	--	--	--
--	--	--	--
--	--	--	--
-186.1	4.0	1590	20
-326.1	4.0	3105	20
-438.3	4.0	4570	25
-392.0	4.0	3930	25

location	year	month	sample type	depth (m)	volume (L)	CF	total (mg)	mgC	µmolC/L	%C recovered
HOT	2014	August	HMW UDOM	7.5	3220	1073	2141	548	14.2	18
HOT	2014	August	HMW UDOM	400	3880	1293	689	171	3.7	8
HOT	2014	August	HMW UDOM	850	3100	1033	806	163	4.4	11
HOT	2014	August	HMW UDOM	2500	4300	1433	865	171	3.3	9
HOT	2015	May	HMW UDOM	7.5	3319	1037	1537	492	12.4	16
HOT	2015	May	HMW UDOM	400	2945	998	770	170	4.8	11
HOT	2015	May	HMW UDOM	850	3330	1189	674	154	3.9	9
HOT	2015	May	HMW UDOM	2500	3939	1358	603	117	2.5	6
BATS	2015	August	HMW UDOM	2	2549	850	1988	327	10.7	11
BATS	2015	August	HMW UDOM	400	2500	833	1513	163	5.4	8
BATS	2015	August	HMW UDOM	850	1170	390	1221	66	4.7	9
BATS	2015	August	HMW UDOM	2500	1750	583	1223	75	3.6	7
BATS	2015	August	HMW UDOM	2500	1750	583	1621	110	5.3	11
BATS	2016	May	HMW UDOM	2	2999	1000	2240	336	9.3	13
BATS	2016	May	HMW UDOM	400	2999	1000	1804	188	5.2	10
BATS	2016	May	HMW UDOM	850	3001	1000	1726	156	4.3	10
BATS	2016	May	HMW UDOM	2500	3007	1074	1659	144	4.0	8

location	year	month	sample type	depth (m)	volume (L)	loading (L/g)	total (mg)	mgC	µmolC/L	%C recovered
HOT	2014	August	LMW SPE-DOM	7.5	796	2.7	257	138	14.5	18
HOT	2014	August	LMW SPE-DOM	400	1050	3.5	312	162	12.9	25
HOT	2014	August	LMW SPE-DOM	850	800	2.7	230	117	12.2	29
HOT	2014	August	LMW SPE-DOM	2500	1000	3.3	248	128	10.7	25
HOT	2015	May	LMW SPE-DOM	7.5	2200	4.4	805	409	15.5	20
HOT	2015	May	LMW SPE-DOM	400	2500	5.0	738	375	12.5	23
HOT	2015	May	LMW SPE-DOM	2500	3180	6.4	806	445	11.7	29
BATS	2015	August	LMW SPE-DOM	2	1500	5.0	791	404	22.4	24
BATS	2015	August	LMW SPE-DOM	400	1500	5.0	640	333	18.5	27
BATS	2015	August	LMW SPE-DOM	850	800	2.7	362	165	17.2	34
BATS	2015	August	LMW SPE-DOM	2500	1000	3.3	366	185	15.4	31
BATS	2016	May	LMW SPE-DOM	2	2000	6.7	1014	508	21.2	29
BATS	2016	May	LMW SPE-DOM	400	2000	6.7	895	428	17.8	34
BATS	2016	May	LMW SPE-DOM	850	2000	6.7	873	423	17.6	39
BATS	2016	May	LMW SPE-DOM	2500	2000	6.7	829	396	16.5	35

C/N	±	$\delta^{13}C$ (‰)	±	CAMS #	Fm	±	$\Delta^{14}C$ (‰)	±	^{14}C age (ybp)	±
12.9	0.06	-22.1	0.05	169865	0.9703	0.0038	-37.3	3.8	240	35
11.9	0.06	-21.5	0.01	169866	0.8160	0.0022	-190.4	2.2	1635	25
13.1	0.03	-21.9	0.05	169867	0.6615	0.0021	-343.7	2.1	3320	30
13.1	0.07	-21.1	0.04	169868	0.6252	0.0018	-379.7	1.8	3775	25
12.3	0.02	-22.5	0.01	172708	0.9575	0.0033	-50.0	3.3	350	30
11.5	0.24	-21.9	0.33	172709	0.8292	0.0029	-177.3	2.9	1505	30
12.2	0.02	-21.5	0.31	172710	0.7188	0.0028	-286.9	2.8	2655	35
12.5	0.12	-21.5	0.06	172711	0.6393	0.0023	-365.7	2.3	3595	30
13.5	0.15	-22.4	0.07	175978	0.9570	0.0032	-43.0	3.2	355	30
11.8	0.06	-21.6	0.05	175979	0.8415	0.0029	-158.5	2.9	1385	30
12.0	0.12	-21.4	0.08	175980	0.7325	0.0022	-267.5	2.2	2500	25
12.5	0.21	-21.3	0.06	175981	0.6958	0.0019	-304.2	1.9	2915	25
12.1	0.15	-21.4	0.04	175982	0.7118	0.0022	-288.2	2.2	2730	25
12.5	0.09	-22.3	0.01	175988	0.9359	0.0031	-64.1	3.1	530	30
11.7	0.09	-21.7	0.04	175989	0.8291	0.0026	-170.9	2.6	1505	30
12.0	0.05	-21.3	0.09	175990	0.7608	0.0022	-239.2	2.2	2195	25
12.5	0.31	-21.3	0.11	175991	0.7349	0.0025	-265.1	2.5	2475	30

C/N	±	$\delta^{13}C$ (‰)	±	CAMS #	Fm	±	$\Delta^{14}C$ (‰)	±	^{14}C age (ybp)	±
28.2	0.26	-22.9	0.06	169869	0.6503	0.0021	-354.8	2.1	3455	30
26.2	0.11	-22.5	0.01	169870	0.5841	0.0017	-420.4	1.7	4320	25
24.2	0.01	-22.2	0.04	169871	0.4858	0.0015	-518.0	1.5	5800	30
26.4	0.21	-22.4	0.09	169872	0.4337	0.0014	-569.7	1.4	6710	30
27.6	0.15	-22.6	0.03	172712	0.6622	0.0023	-343.0	2.3	3310	30
26.1	1.90	-22.7	0.42	172713	0.5657	0.0022	-438.8	2.2	4575	35
28.5	0.03	-22.8	0.06	172715	0.4257	0.0017	-577.6	1.7	6860	35
27.2	0.06	-23.0	0.04	175983	0.6839	0.0020	-316.1	2.0	3050	25
24.7	0.13	-22.7	0.05	175984	0.4922	0.0015	-507.8	1.5	5695	25
21.3	0.25	-22.3	0.09	175985	0.5464	0.0016	-453.6	1.6	4855	25
21.7	0.02	-22.1	0.02	176498	0.5428	0.0016	-461.6	1.6	4910	25
27.1	0.72	-23.1	0.08	175992	0.6664	0.0026	-333.6	2.6	3260	35
25.8	0.02	-22.9	0.00	175993	0.5985	0.0019	-401.5	1.9	4125	30
25.4	0.06	-22.9	0.03	175994	0.5145	0.0019	-485.5	1.9	5340	30
24.6	0.09	-22.8	0.02	175995	0.5912	0.0017	-408.8	1.7	4220	25